

# Searching for massive galaxies at $z \geq 3.5$ in GOODS-North

C. Mancini<sup>1,2,4</sup>, I. Matute<sup>2</sup>, A. Cimatti<sup>3</sup>, E. Daddi<sup>4</sup>, M. Dickinson<sup>5</sup>, G. Rodighiero<sup>6</sup>, M. Bolzonella<sup>7</sup>, L. Pozzetti<sup>7</sup>

<sup>1</sup> Dipartimento di Astronomia e Scienza dello Spazio, Università degli Studi di Firenze, Largo E. Fermi 3 50125, Firenze, Italy  
e-mail: [mancini@arcetri.astro.it](mailto:mancini@arcetri.astro.it)

<sup>2</sup> Osservatorio Astrofisico di Arcetri (OAF), INAF-Firenze, Largo E. Fermi 5, 50125 Firenze

<sup>3</sup> Dipartimento di Astronomia, Università di Bologna, via Ranzani 1, I-40127 Bologna, Italy

<sup>4</sup> CEA-Saclay, DSM/DAPNIA/Service d'Astrophysique, 91191 Gif-Sur Yvette Cedex, France

<sup>5</sup> NOAO, 950 N. Cherry Ave. P.O. 26732, Tucson, AZ 85726-6732, USA

<sup>6</sup> Dipartimento di Astronomia, Università di Padova, Vicolo Osservatorio 2, I-35122, Padova, Italy

<sup>7</sup> INAF-Bologna, Via Ranzani, I-40127 Bologna, Italy

Preprint online version: November 7, 2021

## ABSTRACT

**Aims.** We constrain the space density and properties of massive galaxy candidates at redshifts of  $z \geq 3.5$  in the Great Observatories Origin Deep Survey North (GOODS-N) field. By selecting sources in the *Spitzer* + IRAC bands, a highly stellar mass-complete sample is assembled, including massive galaxies which are very faint in the optical/near-IR bands that would be missed by samples selected at shorter wavelengths.

**Methods.** The  $z \geq 3.5$  sample was selected down to  $m_{AB} = 23$  mag at  $4.5 \mu\text{m}$  using photometric redshifts that have been obtained by fitting the galaxies spectral energy distribution at optical, near-IR bands and IRAC bands. We also require that the brightest band (in AB scale) in which candidates are detected is the IRAC  $8.0 \mu\text{m}$  band in order to ensure that the near-IR  $1.6 \mu\text{m}$  (rest-frame) peak is falling in or beyond this band.

**Results.** We found 53  $z \geq 3.5$  candidates, with masses in the range of  $M_\star \sim 10^{10} - 10^{11} M_\odot$ . At least  $\sim 81\%$  of these galaxies are missed by traditional Lyman Break selection methods based on ultraviolet light. *Spitzer* + MIPS emission is detected for 60% of the sample of  $z \geq 3.5$  galaxy candidates. Although in some cases this might suggest a residual contamination from lower redshift star-forming galaxies or Active Galactic Nuclei, 37% of these objects are also detected in the sub-mm/mm bands in recent SCUBA, AzTEC and MAMBO surveys, and have properties fully consistent with vigorous starburst galaxies at  $z \geq 3.5$ . The comoving number density of galaxies with stellar masses  $\geq 5 \times 10^{10} M_\odot$  (a reasonable stellar mass completeness limit for our sample) is  $2.6 \times 10^{-5} \text{ Mpc}^{-3}$  (using the volume within  $3.5 < z < 5$ ), and the corresponding stellar mass density is  $\sim (2.9 \pm 1.5) \times 10^6 M_\odot \text{ Mpc}^{-3}$ , or about 3% of the local density above the same stellar mass limit. For the sub-sample of MIPS-undetected galaxies, we find a number density of  $\sim 0.97 \times 10^{-5} \text{ Mpc}^{-3}$  and a stellar mass density of  $\sim (1.15 \pm 0.7) \times 10^6 M_\odot \text{ Mpc}^{-3}$ . Even in the unlikely case that these are all truly quiescent galaxies, this would imply an increase in the space density of passive galaxies by a factor of  $\sim 15$  from  $z \sim 4$  to  $z = 2$ , and by  $\sim 100$  to  $z = 0$ .

**Key words.** Cosmology: observation, – Galaxies: formation – Galaxies: evolution – Infrared: galaxies

## 1. Introduction

The question of the galaxy mass assembly at early cosmological epochs is still open. In a  $\Lambda$ CDM Universe, the standard formation scenario predicts hierarchical growth of structures. Local galaxies would have been formed through repeated merging events. The first semi-analytic galaxy-formation models (Kauffmann & Charlot 1998) predicted that the assembly of the most massive systems would only have been completed in the most recent epochs ( $z < 1$ ). Nevertheless, in recent years a substantial population of massive galaxies has been found beyond  $z \sim 1$ . Up to  $z \approx 2.5$  the most massive objects spectroscopically confirmed are similar to the local Early Type Galaxies (ETGs): old (age of  $\sim 1$  Gyr), passively evolving, and with  $M_\star > 10^{11} M_\odot$  (Cimatti et al. 2004; McCarthy et al. 2004; Daddi et al. 2005; Saracco et al. 2005; Kriek et al. 2006).

At higher redshifts the availability of multi-wavelengths data from the new generations of deep surveys has allowed searches for massive galaxy candidates up to  $z \approx 5 - 6.5$ . The dropout-technique pioneered by Steidel et al. (1996) to find Lyman-

break galaxies (LBGs) at  $z \approx 3$ , has proven successful also for identifying blue star-forming galaxies at higher redshifts ( $z \sim 4 - 6$  Steidel et al. 1999; Dickinson 1998; Steidel et al. 2003; Giavalisco et al. 2004b; McLure et al. 2006; Yan et al. 2006).

A substantial amount of spectroscopic confirmations is available for LBGs at  $z \sim 5 - 6$  (Bunker et al. 2003; Stanway et al. 2004; Dickinson et al. 2004; Eyles et al. 2007; Stark et al. 2007; Vanzella et al. 2008). This allowed early estimates of the stellar mass density at those redshifts. For instance Yan et al. (2006) measured the comoving stellar mass density at  $z \sim 6$  in the total GOODS field and found it in good agreement with the simulations of Night et al. (2006). The stellar mass density found in the GOODS-S field by Eyles et al. (2007) for a sample of i-dropout LBGs in the same redshift range is also consistent with the Yan et al. (2006) results. However it is larger by a factor of 4 ( $\sim 2$ , if the different IMFs are taken into account) with respect to the Bower et al. (2006) semi-analytical model predictions. The general picture is, however, still controversial and further studies are necessary to better constrain galaxy formation models. In fact, the Lyman-break technique can only be used

to select actively star-forming galaxies having sufficiently luminous UV emission to allow their detection and color selection. Galaxies, and especially massive ones, could be faint or undetected in the optical and near-infrared bands. Such sources could be either old systems with small quantities of dust and low levels of star-formation rate, or dust reddened starburst galaxies. If such  $z > 3.5$  objects really exist, they would be too faint to be studied spectroscopically with the instrumentation that is currently available, and the only possible approach that can be used to constrain their number density and their properties remains a photometric one, based on the Spectral Energy Distribution (SED) fitting analysis.

The most popular criterion used so far to select high- $z$  galaxies with red rest-frame colours is based on the redshifted 4000 Å/Balmer break, i.e. the typical features of galaxies with evolved stellar populations. It was pioneered by Franx et al. (2003) to pick out ‘distant red galaxies’ (DRGs) at  $z > 2$  ( $J_s - K_s > 2.3$ , AB system). Recently it was extended by Brammer & van Dokkum (2007) to identify DRGs up to  $z \sim 3.7$  ( $H - K > 0.9$ , AB system). By comparing the properties and the space density of DRGs at  $z \sim 3.7$  and  $z \sim 2.4$  in the same field, they found a stellar mass density of about a factor of 5 lower in the higher redshift bin.

In the recent years the availability of *Spitzer* data has also enabled us to search for galaxies with red rest-frame optical colors at high redshifts, and to better constrain their stellar masses (Fontana et al. 2006; Dunlop et al. 2007; Rodighiero et al. 2007; Wiklind et al. 2008; Eyles et al. 2005). Some of the objects identified may be among the most massive stellar systems found at  $z \sim 4 - 5$ . In particular, Rodighiero et al. (2007) extracted a *Spitzer*+IRAC selected sample in the GOODS-South field, limited to galaxies undetected in the optical and close to the detection limit in the  $K$ -band. Their criterion is complementary with respect to those adopted by previous studies (i.e. the  $K < 23.5$  selection used by Dunlop et al. 2007) and is aimed at identifying high- $z$  massive galaxies that are missed by conventional selection techniques based on optical and near-IR observations. They found a potential population of optically obscured massive galaxies at  $z \geq 4$ . In the same field Wiklind et al. (2008) found 11  $K$ -selected  $z \geq 5$  massive and evolved galaxy candidates. They selected these objects by applying color criteria aimed at the identification of the 4000 Å/Balmer break between the  $K$  and  $3.6 \mu\text{m}$  passbands, in combination with SED fitting.

It should be noted that in both of these works roughly half of the high- $z$  massive candidates are detected at  $24 \mu\text{m}$ . The  $24 \mu\text{m}$  emission might be due to obscured AGN activity at high redshift, but also from Polycyclic Aromatic Hydrocarbon (PAH) emission in dusty star forming galaxies at lower redshifts. In fact, one has to take into account the degeneracy between reddening and redshift while selecting high redshift sources based on photometry. Recent studies of sub-mm galaxies (SMGs) have shown that moderate  $24 \mu\text{m}$  emission can arise from massive starburst galaxies at high redshift ( $z \geq 3.5$ , Daddi et al. 2008; Greve et al. 2008; Perera et al. 2008). Hence one of the main difficulties in selecting bona fide high- $z$  galaxies through photometric redshifts is to efficiently remove the contamination from dust-reddened galaxies at lower redshift. As an example, one of the most debated cases is the galaxy HUDF-JD2 in the Hubble Ultra Deep Field. Mobasher et al. (2005) suggested that such a galaxy is a massive ( $M \approx 6 \times 10^{11} M_\odot$ ), low-reddened, old galaxy (with an age of  $\sim 10^8$  yrs and a  $z_{\text{form}} > 9$ ) at  $z \approx 6.5$ . However, other studies (e.g. Dunlop et al. 2007; Rodighiero et al. 2007; Chary et al. 2007) suggest that HUDF-JD2 is instead a lower redshift

galaxy with very strong dust reddening ( $z \approx 2.2$  and  $A_V \approx 3.8$ , Dunlop et al. 2007).

The principal aim of this paper is to study the properties and space density of massive galaxies at  $z \geq 3.5$  in the Great Observatory Origin Deep Survey-North (GOODS-N). This survey is especially suitable for our purpose because of the quality and depth of the available multi-wavelength data. In particular it has the advantage of a better coverage at sub-millimetric wavelengths with respect to GOODS-S. In addition, while similar searches have been carried out in the GOODS-South field, none has been performed so far in the northern hemisphere field of the GOODS Survey. We chose to select the sample in the IRAC channel 2 ( $4.5 \mu\text{m}$ ) for two reasons. First, to pick out the most massive systems. At  $z \geq 3.5$  the  $4.5 \mu\text{m}$  band samples the rest-frame near-IR emission, which is well correlated to the galaxy stellar mass (Kauffmann & Charlot 1998). Second, the  $4.5 \mu\text{m}$  band selection allows us to have a more complete sample with respect to an optical or near-IR selection. This is one of the main differences with the previous works: we attempted to construct a sample as complete as possible, including objects undetected in optical and near-IR bands, and hence missed by the optical or  $K$  selection criteria used so far in the literature (Drory et al. 2004; Fontana et al. 2006; Dunlop et al. 2007; Wiklind et al. 2008; Brammer & van Dokkum 2007). As already mentioned, Rodighiero et al. (2007) also used an IRAC band ( $3.6 \mu\text{m}$ ) selection, but their additional conditions about the lack of optical emission and the faint near-IR detection ( $K > 23$ , AB system) make their sample incomplete by construction.

The structure of the paper is as follows. In Sect. 2 we present the optical, near-IR and IR data available for the GOODS-N field. In Sect. 3 we describe the IRAC selection and the photometry of the sample. Sect. 4 describes the results from the SED fitting analysis with the measurement of photometric redshift and the stellar mass estimates. In Sect. 5 we discuss the selection of  $z \geq 3.5$  galaxy candidates. In the same section we discuss the detections of the sample in the MIPS-24  $\mu\text{m}$  and in the sub-mm/mm. In Sect. 6 we study the effects of incompleteness and the bias against low mass galaxies in our magnitude-limited sample. We give estimates for the comoving number density and stellar mass density for the full sample, and for the sub-sample of MIPS-undetected galaxies. Sect. 7 presents the summary and conclusions.

Throughout this paper, we adopt the following cosmological parameters  $H_0 = 70 \text{ km s}^{-1} \text{ Mpc}^{-1}$ ,  $\Omega_\Lambda = 0.7$  and  $\Omega_m = 0.3$ , and all magnitudes are given in the AB system.

## 2. The GOODS-N data.

This work is based on the analysis of the Great Observatory Origins Deep Survey - North (GOODS-N) data. The GOODS-N is a multi-wavelength deep survey centered in the Hubble Deep Field North (HDFN  $12^{\text{h}}36^{\text{m}}55^{\text{s}}, +62^\circ 14' 15''$  Giavalisco et al. 2004b) with size of  $\sim 10' \times 16'$ . The field is part of the GOODS *Spitzer* Legacy Program (PI: M. Dickinson) and the *Hubble Space Telescope* (HST) Treasury Program (PI: M. Giavalisco), divided in two fields (GOODS-N and GOODS-S), from the northern and southern hemispheres (see Dickinson et al. 2003). The GOODS-N field observations span from the X-rays to the sub-mm wavelengths. In particular, for the analysis presented in this paper, we make use of the following data sets:

- $U$  band imaging, taken at the Kitt Peak National Observatory (KPNO) 4m telescope, from the Hawaii Hubble Deep Field North (H-HDFN) survey datasets (Capak et al. 2004).

- Optical imaging from the *Hubble Space Telescope* (HST) with the Advanced Camera for Survey (ACS) in the F435W (*B*), F606W (*V*), F775W (*i*), F850LP (*z*) pass-bands (Giavalisco et al. 2004b).
- Near-Infrared imaging, in the *J*, *H* and *Ks* bands, from the KPNO-4m telescope (M. Dickinson private communication).
- Infrared observations from the *Spitzer* Space Telescope (Werner et al. 2004) + Infra-Red Array Camera (IRAC; Fazio et al. 2004)
- 24  $\mu\text{m}$  observations from the *Spitzer* Space Telescope and Multi-band Imaging Photometer for *Spitzer* (MIPS; Rieke et al. 2004).

Specifics of the data are given below.

### 2.1. KPNO 4m U-band imaging

The H-HDFN Survey is a deep multi-colour imaging survey of  $0.2 \text{ degrees}^2$ , centered in the Hubble Deep Field North. The data consist of deep images in the U, B, V, R, I, and  $z'$  bands. Out of these we used only the U-band images, due to the availability of HST/ACS imaging from the *B* through *z* bands. The U-band observations were taken in March 2002, using the KPNO-4m telescope with the MOSAIC prime focus camera (Muller et al. 1998), covering a field of view of  $36' \times 36'$  with a seeing of  $1''.26$ . We analyzed the part overlapping with the GOODS-N field (an area of about  $165 \text{ arcmin}^2$  around the HDF-N). The U image reaches a  $5\sigma$  sensitivity limit of 27.1 mag.

### 2.2. ACS+HST optical imaging

The GOODS-N optical data from the Advanced Camera for Surveys (ACS), on-board HST, are in the F435W (*B*), F606W (*V*), F775W (*i*), F850LP (*z*) pass-bands (v1.0 data products). The  $5\sigma$  point source sensitivity limits are 28.5, 28.8, 28.1, 27.6 respectively, scaled from values reported in Giavalisco et al. (2004b) to the full exposure time of ACS v1.0 images. The HST/ACS high-resolution data is organized in 17 images, called “sections”. Each section is an image  $8192 \times 8192$  pixels in size, drizzled from the native ACS pixel scale ( $0''.05/\text{pixel}$ ) to an image subsampled at  $0''.03/\text{pixel}$ . The huge size ( $\sim 40000 \times 40000$  pixels) of the combined HST images in the field made source extraction an extremely intensive computing task. Therefore we re-binned the final image using an  $8 \times 8$  pixel kernel, requiring flux conservation. The new re-binned mosaic obtained in this way has a size of  $5120 \times 5120$  pixels, and a pixel scale of  $0''.24/\text{pixel}$ .

### 2.3. KPNO 4m FLAMINGOS near-infrared imaging

We complemented the public data with near-IR imaging taken at the KPNO-4m telescope with the Florida Multi-object Imaging Near-IR Grism Observational Spectrometer (FLAMINGOS; observations by Mark Dickinson et al.). The FLAMINGOS images in the *J*, *H* and *Ks* pass-bands, are mosaics of data taken at different pointings and orientations to cover the whole GOODS-N. The average exposure times per band in the main part of the GOODS-N area are 20250 s, 15770 s and 35440 s at *J*-, *H*- and *Ks*, respectively. The three images reach a  $5\sigma$  point source sensitivities of 24.03, 23.77, 23.81 mag. The pixel-scale is  $0''.316/\text{pixel}$ , and the seeing  $1''.27$ ,  $1''.2$  and  $1''.2$ , for the *J*, *H*, and *Ks* pass-bands, respectively.

We performed some photometric checks before measuring source fluxes. We verified the zero-points reliability of

FLAMINGOS images, comparing the bright and unsaturated star magnitudes with stars from the 2MASS catalogue.

### 2.4. Spitzer imaging at 3.6 to 24 $\mu\text{m}$

The infrared imaging is from *Spitzer* Space Telescope + IRAC between 3.6 and  $8.0 \mu\text{m}$ , and from *Spitzer* + MIPS at  $24 \mu\text{m}$ .

The four IRAC channels, centered on 3.6  $\mu\text{m}$ , 4.5  $\mu\text{m}$ , 5.8  $\mu\text{m}$ , 8.0  $\mu\text{m}$ , have formal  $5\sigma$  limits for isolated point sources of 26.1, 25.5, 23.5, 23.4 respectively. The mean FWHM of a point source for the IRAC-bands are  $1''.66$ ,  $1''.72$ ,  $1''.88$  and  $1''.98$ , for channels 1, 2, 3 and 4 respectively. The initial image pixel-scale of  $1''.22$  is reduced to  $0''.6/\text{pixel}$ , after the dithering and drizzling process.

The MIPS public dataset includes calibrated maps and a catalogue of 24  $\mu\text{m}$  sources with flux densities  $S_{24} > 80 \mu\text{Jy}$ . The PSF was generated from isolated sources in the image, and renormalized based on the aperture correction published in the MIPS data Handbook (v2.1, section 3.7.5, table 3.12). Then an independent PSF algorithm was run to extend the 24  $\mu\text{m}$  sample to fainter sources (see Rodighiero et al. 2006). By this procedure the detection threshold was extended to  $S_{24} > 35 \mu\text{Jy}$ . Since the 24  $\mu\text{m}$  information can help to better constrain the SFR (Chary & Elbaz 2001) and the nature of high-redshift sources, we also exploited a deeper 24  $\mu\text{m}$  catalogue, reaching a  $5\sigma$  limit of  $20 \mu\text{Jy}$  (Chary et al. 2008 in preparation, Daddi et al. 2007).

## 3. Sample selection

In order to have an accurate measurement of the object fluxes in all bands, we performed aperture photometry in each band using the *SExtractor* software (Bertin & Arnouts 1996). The initial catalogue was built by selecting the sources in the 4.5  $\mu\text{m}$  public image obtained with *Spitzer* Space Telescope + IRAC, down to a limiting magnitude of  $m_{4.5} = 23.0$  ( $2.3 \mu\text{Jy}$ ). Simulations indicate that a sample selected in this way is complete at the 80% level at  $m_{4.5} \sim 23.0$  (M. Dickinson private communication), where 20% of the sources are lost due to blending.

The infrared selection allows us to search for the presence of massive galaxies up to very high redshifts. In fact for galaxies at  $3.5 < z < 7$  the rest-frame light emitted at  $\lambda > 0.6 \mu\text{m}$  is redshifted into the IRAC 4.5  $\mu\text{m}$  band. Therefore, the 4.5  $\mu\text{m}$  selection is directly sensitive to stellar mass, rather than to the ongoing star formation activity. From a technical point of view, the choice of selecting the sample at 4.5  $\mu\text{m}$  represents the best compromise amongst the IRAC bands in terms of image quality, blending problems, and sensitivity.

In order to detect galaxies in the 4.5  $\mu\text{m}$  IRAC band and perform the photometry we used *SExtractor* with the following set of parameters. The detection limit was set at  $\sim 1\sigma$  above the sky background. A Gaussian filter was used to improve the detection of faint extended objects. Due to the high crowding of IRAC images, and the large PSF, the minimum contrast parameter was set to a small value of  $5 \times 10^{-9}$ , to help with source deblending.

We measured fluxes in  $4''.0$  diameter apertures, as this size allows us to minimize uncertainties in the photometry in the *Spitzer* +IRAC bands (as also suggested by the SWIRE team<sup>1</sup>). In the 4.5  $\mu\text{m}$  IRAC filter we applied an aperture correction of 0.25 mag that we independently computed from point-source objects, by measuring the total flux in  $8''.0$  diameter apertures.

The final IRAC selected catalogue contains 4142 objects ( $m_{4.5} < 23.0$ ).

<sup>1</sup> [http://data.spitzer.caltech.edu/popular/swire/20050603\\_enhanced\\_v1/](http://data.spitzer.caltech.edu/popular/swire/20050603_enhanced_v1/)

### 3.1. Multi-band Photometry

We searched for the counterparts of the 4 142 IRAC-selected objects in the other datasets. We detected the sources and measured the photometry independently in each dataset and associated counterparts to the  $4.5 \mu\text{m}$  IRAC detected galaxies using a search radius of  $1''.0$ .

For the U-band we measured fluxes  $4''.0$  (diameter) apertures. We applied an aperture-correction of 0.1 mag, computed by considering the total flux in  $8''.0$  diameter aperture. For undetected sources we used the  $3\sigma$  flux upper limit of 26.7 mag. This value was computed by measuring the standard deviation of the sky signal at random position over the field.

For the HST/ACS bands circular apertures with diameters of  $2''.0$  were used. The following aperture-corrections for point-sources were found by measuring the total flux in  $5''.0$  diameter-aperture, for the B, V, i, z bands: 0.050, 0.040, 0.030, 0.045 mag, respectively. For undetected objects we obtained  $3\sigma$  upper limits in the same way as described above for the U-band. We measured upper limits to be 26.3, 26.9, 26.3, 25.5, for the B, V, i and z bands respectively.

The near-IR magnitudes were measured in  $4''.0$  diameter apertures, and corrected to total (within  $8''.0$  diameter) by 0.1, 0.14, 0.15 mag for the J-, H- and Ks- band, respectively. The  $3\sigma$  detection limits are 23.3, 23.0 and 23.1, for the J-, H- and Ks-band.

In the other IRAC channels we used the same aperture diameters as in IRAC- $4.5 \mu\text{m}$  ( $4''.0$ ), and the same approach to compute aperture corrections. The final IRAC magnitudes were obtained by applying aperture corrections of 0.23, 0.25, 0.40, 0.44 mag for 3.6, 4.5, 5.8 and  $8.0 \mu\text{m}$  bands, respectively.

To check the reliability of our photometry we compared the colors of stars with those expected based on the models of Lejeune et al. (1997) in color-color diagrams involving one band from each one of the three datasets (ACS/HST optical, Near-Infrared/FLAMINGOS and infrared/IRAC-*Spitzer*). The case of  $(b - J)$  vs  $(J - m_{3,6})$  is shown in Fig. 1. The star sequence is clearly visible on the left side of the panel. As it appears from the figure we found a very good agreement between the observed colours (green circles) and the expected ones (red asterisks from the “corrected” templates of Lejeune et al. 1997) for spectroscopically identified stars (public database of the TKRS survey Wirth et al. 2004). Therefore, thanks to the very good concordance between optical, near-IR and IR datasets we did not have to apply further photometric corrections to our data magnitudes.

The photometric errors given by *SExtractor* software are generally underestimated, because the software does not take into account the possible correlation between neighboring pixels that can result from image processing. Hence we applied corrections to the photometric errors in each data-set. For the four IRAC channels we added 0.1 mag quadratic to *SExtractor* errors. This is a conservative choice to account for uncertainties on the photometric zeropoints and on the aperture corrections, as also suggested in Maraston et al. (2006). In the other filters we measured the signal in a number of random sky positions in the field, within the same aperture used to perform galaxy photometry in each band. Comparing the standard deviation of these measurements to the actual errors in the photometry of faint galaxies inferred by *SExtractor* we derived scaling factors to apply to the formal errors reported in the *SExtractor* catalogues.

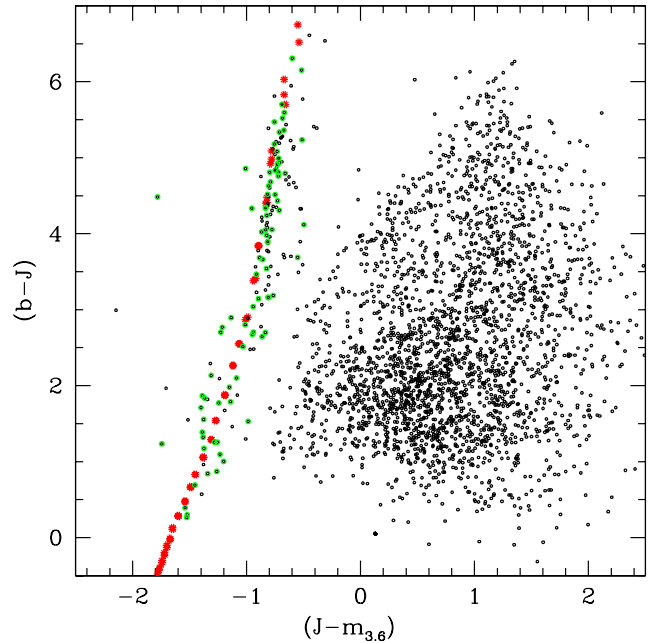


**Fig. 1.** The color-color diagram  $(b - J)$  vs  $(J - m_{3,6})$ . The star sequence is clearly visible on the left side of the diagram. We found a very good agreement between the observed colours (green circles) and the expected ones (red asterisks from the “empirically corrected” templates of Lejeune et al. 1997) for spectroscopically identified stars (public database of the TKRS survey Wirth et al. 2004).

## 4. Spectral Energy Distribution (SED) fitting analysis

### 4.1. Photometric redshifts estimate

To estimate the photometric redshifts of our sample of galaxies we used the *Hyperz* code (Bolzonella et al. 2000). This code compares the multi-wavelength photometry of each source to a database of theoretical and/or empirical templates at different redshifts. The best fit solution, for a given set of templates, is derived through a standard  $\chi^2$  minimization.

For the determination of the photometric redshifts we excluded the  $24 \mu\text{m}$  band, because the templates of stellar populations that we used do not include dust emission. For a similar reason we decided to omit also the  $8 \mu\text{m}$  band, which includes thermal dust and PAH (i.e. non-stellar) emission for the lower redshift galaxies and can be contaminated by star formation or AGN also at higher redshift (Daddi et al. 2007). We used the template library of the observed SED constructed by Coleman et al. (1980, hereafter CWW), extended in the UV and IR regions by means of Bruzual & Charlot (2003) synthetic spectra, as explained in the *Hyperz* User’s manual<sup>2</sup>. This set of templates includes four types of spectra with characteristics corresponding to the different local types of galaxies: Elliptical/Lenticular (E/S0), Spiral (Sbc and Scd) and Irregular (Im). The CWW library was complemented with a spectrum of a Young Star-Burst (SB) galaxy, with constant star formation rate (SFR) and age of 0.1 Gyr, from the Bruzual & Charlot (2003) models.

We took into account the dust extinction by applying the Calzetti et al. (2000) law. The extinction parameter ( $A_V$ ) was allowed to vary from 0 to 0.8 in steps of  $d(A_V) = 0.1$ . Only a small range of  $A_V$  was allowed since the CWW templates include al-

<sup>2</sup> <http://webast.ast.obs-mip.fr/hyperz/>

ready intrinsically reddened SEDs. The permitted redshift range span the large interval of values of  $0 < z < 10$ , with a step of  $d(z) = 0.07$ .

We used the prescription of Madau (1995) to represent the average Lyman- $\alpha$  forest opacity as a function of wavelength and redshift.

#### 4.2. Photometric redshift reliability

We checked the reliability of our photometric redshifts for 836 objects of the GOODS-N field having high quality spectroscopic redshifts. Unobscured AGN were excluded from the list by means of the X ray information from the publicly available X-ray catalogue of the Chandra Deep Field-North Survey Alexander et al. (2003). The largest number of spectroscopic redshifts (721) are from the public database of the Team Keck Treasury Redshift Survey (TKRS; Wirth et al. 2004), and are accurate to  $100 \text{ km s}^{-1}$ . The median redshift of this survey is rather low ( $z = 0.65$ ). In order to increase the number of available objects with the highest spectroscopic redshifts, we complemented the TKRS database with the galaxies found by Reddy et al. (2006) in the redshift interval of  $2.0 \leq z \leq 3.5$  (108). We also used some objects (5) up to  $z \approx 5$  from the NASA/IPAC Extragalactic Database<sup>3</sup> (NED).

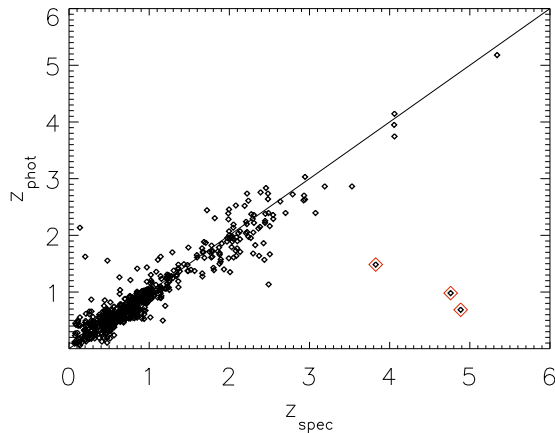


**Fig. 2.** Comparison between photometric  $z_{phot}$  and spectroscopic  $z_{spec}$  redshifts for 836 objects of our sample. The  $z_{spec} - z_{phot}$  relation has a combined mean offset of  $(z_{spec} - z_{phot}) / (1 + z_{spec}) = 0.004$  with an rms scatter of  $\sigma [(z_{spec} - z_{phot}) / (1 + z_{spec})] = 0.09$ . For the flagged objects (red open diamonds), appearing as catastrophic outliers we suggest the lower redshift solution, as detailed in the text.

The comparison between photometric ( $z_{phot}$ ) and spectroscopic ( $z_{spec}$ ) redshifts is shown in Fig.2. After clipping  $5 \sigma$  outliers we found a combined mean offset of  $(z_{spec} - z_{phot}) / (1 + z_{spec}) = 0.004$  and a rms scatter of  $\sigma [(z_{spec} - z_{phot}) / (1 + z_{spec})] = 0.09$ . This result was obtained by means of an iterative optimization procedure applied to the *Hyperz* results. It consists in repeating the SED fitting analysis for the same objects, fixing the redshifts to the known spectroscopic values. For each filter the median offset between empirical and “theoretical” magnitudes (the latter deriving from the best fit SEDs) was obtained. The largest photometric offsets that we found were for the *U*-, *z*- and *K*-bands (+0.2, +0.09, +0.14, respectively) and  $|\Delta mag| \sim 0.05$

**Table 1.** Outliers of our  $z_{phot} - z_{spec}$  comparison (Fig. 2). Their best fit SEDs are shown in Fig. 3. The coordinates and the spectroscopic redshifts are from NED database. The last column is the distance to the NED position (arcsec).

id	RA	Dec	$z_{phot}$	$z_{spec}$	dist(″)
#6955	12:36:40.510	+62:13:34.90	1.48	3.826	0.27
#8734	12:36:37.630	+62:14:53.70	0.68	4.886	0.16
#8903	12:37:21.048	+62:15:01.73	0.98	4.762	0.41

for the others. Adding these corrections to the observed magnitudes, the rms of the  $\Delta z / (1 + z_{spec})$  quantity was slightly reduced. The same offsets were finally applied to the whole sample for estimating the photometric redshifts.

Since the current work is focused on galaxies at  $z \geq 3.5$  we have carefully examined three outliers (#6955, #8734 and #8903) in the photometric-spectroscopic redshift comparison with reported  $z_{spec} \geq 3.5$ . These are noted with red diamonds in Fig. 2, and information about them is presented in Tab. 1. In Fig. 3 we show the photometric SEDs for these three objects and in Fig. 4 we show cutout images from *U*-band through  $24 \mu\text{m}$ . For the first two objects (#6955 and #8734) Dawson et al. (2001) report Keck spectra showing isolated emission lines with no continuum detection (their quality class 4; see Tab. 2 and 3 of that paper), which they identify as weak Ly- $\alpha$  emission. However object #6955 is detected at a significance  $> 3 \sigma$  limit in the *U*-band, ruling out the proposed  $z = 3.826$ . More recent Keck/DEIMOS spectra from 2005 and 2006 (M. Dickinson & D. Stern, private communication) detected an emission line at  $9273 \text{ \AA}$  which is likely to be [OII] $3727 \text{ \AA}$  at  $z = 1.488$ , consistent with our photometric redshift estimate for this object. Object #8734 shows a red point source in the HST/ACS images, along with faint, bluer, extended emission to the southeast. This is very likely to be a superposition of a cool galactic star with a faint galaxy. Cowie et al. (2004) report that this is a star based on DEIMOS spectroscopy. The faint, extended component is certainly a galaxy, although it is clearly detected in the ACS *B*-band image, and is therefore unlikely to be at  $z = 4.887$  as reported by Dawson et al. (2001). Overall, the photometry at all wavelengths redward of the *V*-band is dominated by the point source component, and the photometric SED for this object Fig. 3 clearly resembles that of a cool, late-type star (probably an M-dwarf). Finally, for object #8903, Dawson et al. (2001) report  $z = 4.762$ . However, ACS *V - i* and *i - z* colors for this galaxy are not consistent with it being a *V*- dropout Lyman break galaxy, and fall within the locus of ordinary foreground galaxies. The ACS color images show a faint, red, early-type galaxy, and our photometric redshift estimate is  $z_{phot} = 0.89$ , very close to that proposed by Capak et al. (2004). Although Cowie et al. (2004) do not report details about the spectral features that they observed, it is possible that faint [OII] emission at  $z = 0.88$  was mistaken for faint Ly $\alpha$  at  $z = 4.76$ .

#### 4.3. Galaxy mass estimate

We used the code *Hyperzmass* to estimate the mass for each of our sources. The *Hyperzmass* code works in a similar way to *Hyperz* (see Pozzetti et al. 2007). In this task the redshifts were fixed at the derived photometric values, or spectroscopic ones, when available. The observed data points were fitted using both the synthetic spectral models of Bruzual & Charlot (2003, hereafter BC03) and Maraston (2005, hereafter MA05). Both tem-

<sup>3</sup> <http://nedwww.ipac.caltech.edu/>

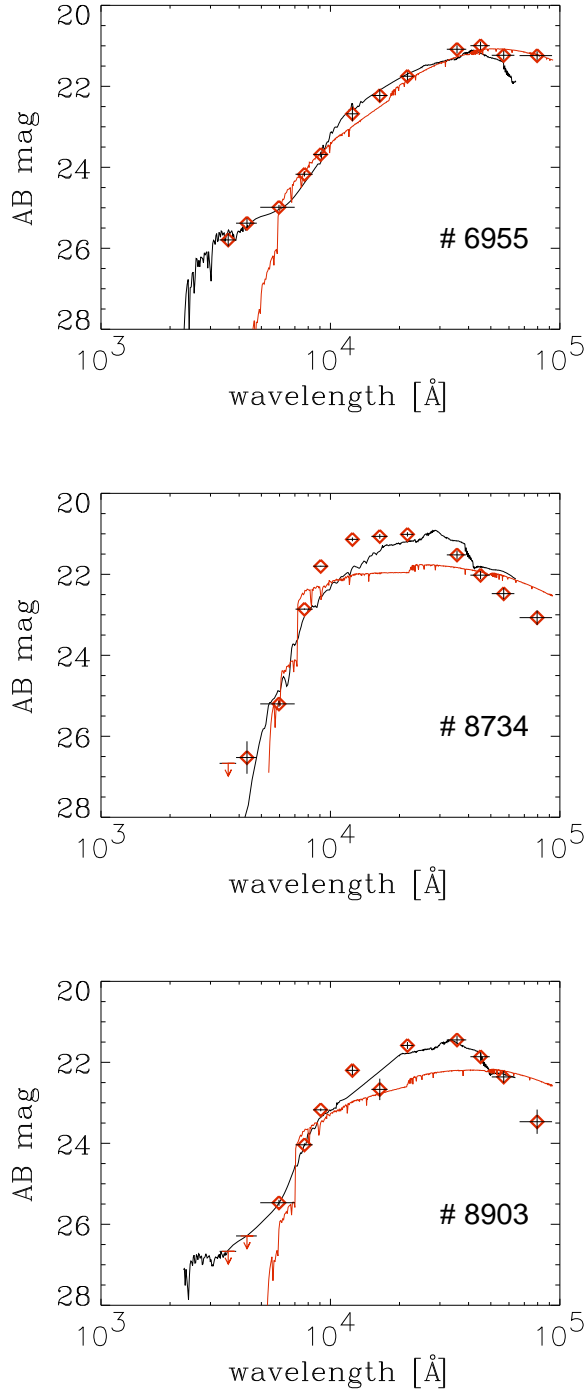


**Fig. 3.** SEDs of the outliers in the  $z_{spec}$ - $z_{phot}$  space (see objects flagged in Fig. 2). Our best fits (black curves) produce photometric redshifts of  $\sim 1.48$ ,  $0.68$  and  $0.98$ , respectively. We compare these results with the best fits (red curves) obtained by fixing the redshifts to the spectroscopic values taken from the literature ( $z = 3.826$ ,  $z = 4.886$ , and  $z = 4.762$ ; NED database). Obviously, the black curves fit the observed data better than the red ones. See also Tab.1

plate sets are composed by models of stellar populations with Star Formation Rates (SFRs) exponentially decreasing with time ( $\psi(t) = \tau^{-1} \exp^{-t/\tau}$ ). In our analysis we considered models with different values of the time-scale  $\tau$  (in unit of Gyr) : 0.1, 0.3, 1,

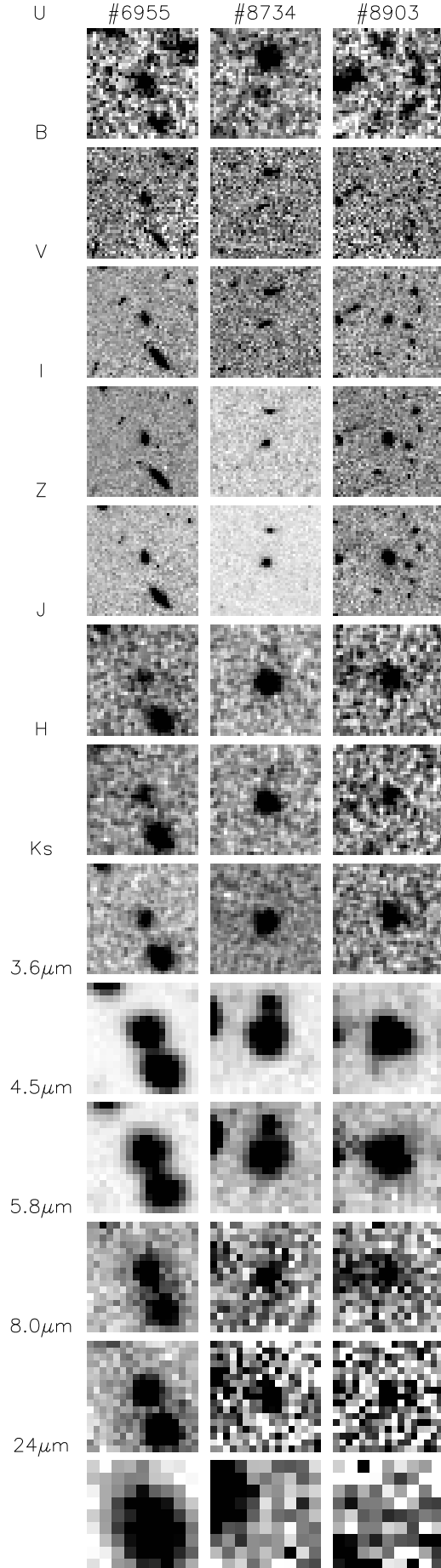


**Fig. 4.** Multi-wavelength identification of the three outlier objects in the  $z_{spec}$ - $z_{phot}$  diagram. The cut-outs have a size of  $10'' \times 10''$ . North is up, East is at left.

2, 3, 5, 10, 15, 30 and  $\infty$ . The last model corresponds to a stellar population with a constant SFR.

For the BC03 models we used the Chabrier (2003) Initial Mass Function (IMF). Instead, the MA05 models adopt the Kroupa (2001) IMF, which is relatively similar to the Chabrier IMF. To compare the different results we computed a systematic correction to convert the masses obtained with Kroupa IMF to Chabrier IMF ( $\log M_{\text{Chabrier}} = \log M_{\text{Kroupa}} - 0.04$ ).

In the SED fitting analysis the extinction parameter,  $A_V$ , was allowed to span the range of values  $0 \leq A_V \leq 6$ , with a step of 0.1. This large reddening range is required given that synthetic stellar population models are not intrinsically reddened as the observed ones. We used  $A_V = 6$  as an upper limit for the reddening, since there is no evidence of objects with  $A_V$  higher than  $\sim 5$ . The galaxy age was left as a free parameter, spanning the range from  $5 \times 10^6$  yr to  $11.7 \times 10^9$  yr (and always requiring ages less than the age of the Universe at each redshift). To minimize the number of free parameters we limited the fits to solar metallicity.

## 5. Massive galaxies at $z \geq 3.5$

As previously discussed, evidence for populations of massive galaxies at  $z > 3$  has been found by several studies. However, results are not yet conclusive since the number of objects is low, and frequently biased against objects that are faint or undetected in optical and near-IR bands. Moreover for most of these objects no spectroscopic redshift information is available. Also, the possible contamination by lower redshift interlopers is a source of uncertainty. To shed some light on the nature and the number density of the high redshift population of massive galaxies we selected a final sample of  $z_{\text{phot}} \geq 3.5$  candidates, by applying the following selection criteria (summarized in Table 2). Among the initial 4 142 IRAC-4.5  $\mu\text{m}$  selected galaxies we found 190 galaxies with photometric redshifts of  $z_{\text{phot}} \geq 3.5$ .

All such objects were carefully inspected for possible blending issues. One of the main problems in using *Spitzer* data in crowded fields is, in fact, the blending between nearby sources. Neighboring objects that can be well separated in optical and near-IR images, might happen to be blended in the IRAC bands, due to the limited spatial resolution of the *Spitzer* telescope. Hence, in order to build a bona-fide sample of high- $z$  galaxies we had to take into account that a fraction of the IRAC-selected objects could be affected by blending. We decided to visually inspect all the  $z \geq 3.5$  objects, and we excluded from the sample any sources that the *SExtractor* software was not able to deblend. To identify them we visually inspected examined the *SExtractor* ‘‘aperture image’’ in each filter. This is a ‘check-image’ given as output by the software, where the circular apertures are shown for all the objects detected above the threshold level. We classified an object as blended if the IRAC position did not correspond to a single source in the higher resolution optical and/or near-IR images (e.g. objects that are well separated in the optical or near-IR images may be blended in the IRAC images due to their poorer angular resolution). About the 25% of the pre-selected  $z_{\text{phot}} \geq 3.5$  objects were flagged as blended and therefore discarded.

By matching our catalogue with the publicly available X-ray catalogue of the Chandra Deep Field-North Survey<sup>3</sup>, we found 14 objects that were detected in the hard X-ray band, and one with soft X-ray flux. We excluded these 15 sources from the final sample since X-ray emission indicates the presence of AGNs in those galaxies, that can alter the observed flux and induce an overestimate of the stellar masses.

Finally we introduced a further criterion, based on IRAC colours. We considered as genuine  $z \geq 3.5$  candidates only those sources showing an SEDs peak at the 8.0  $\mu\text{m}$  observed frame (1-2  $\mu\text{m}$  rest-frame for  $z \geq 3.5$  galaxies) in the AB scale. The reason is that the near-infrared emission of all but extremely young galaxies show a distinct peak at 1.6  $\mu\text{m}$  in the rest-frame, that is redshifted in the 8.0  $\mu\text{m}$  IRAC band for  $z \geq 3.5$  sources. This peak corresponds to the combination of the Planck spectral peak of cool stars and the effects of a minimum in the  $H^-$  opacity in the stellar atmospheres. It has been used as photometric redshift indicator in several previous studies (e.g. Sawicki 2002; Berta et al. 2007). This criterion was applied because at this step we expect that our high- $z$  sample will be contaminated by a substantial fraction of lower-redshift galaxies, because of the intrinsic uncertainty of the photometric redshift estimate. The degeneracy between reddening and redshift could introduce lower-redshift contaminants in the final high- $z$  sample (i.e. dust reddened galaxies at lower redshift can be mistaken for higher- $z$  old stellar populations). Given that galaxies at  $z \geq 3.5$  represent only a minority ( $\sim 4\%$ ) of the galaxy sample selected at 24 $\mu\text{m}$ , while most of the objects are at  $z < 2$ , from a statistical point of view we could expect a more substantial contamination by lower- $z$  sources entering our  $z > 3.5$  redshift selection, largely overbalancing the number of genuine  $z > 3.5$  galaxies lost as due to errors in their photometric redshifts. In addition, as already pointed out, the 8  $\mu\text{m}$  data-point was excluded from the SED fitting analysis because for objects at  $z < 1.8$  it could sample the PAH emission lines for dusty galaxies, and the stellar population models that we used do not include dust emission. In this way, by excluding the 8  $\mu\text{m}$  band from the fitting procedure, we may fail to distinguish galaxies at  $z \sim 2-3$  where the 1.6  $\mu\text{m}$  peak lies in the 5.8  $\mu\text{m}$  band from those at  $z > 3.5$ . Requiring the SED to rise from 5.8 to 8  $\mu\text{m}$  can help to exclude these possible lower-redshift contaminants.

The parameterization of the colour criterion we used is the following:

$$(m_{8.0} \leq m_{5.8} + 0.1) \cap (m_{8.0} \leq m_{4.5} + 0.1) \cap (m_{8.0} \leq m_{3.6} + 0.1) \quad (1)$$

the 0.1 mag terms are introduced to account for the median uncertainty in the IRAC photometry of  $\sim 0.1$ .

In the two panels of Fig. 5 we show the expected  $m_{5.8} - m_{8.0}$  colour as a function of redshift for different stellar population models. The top panel shows Simple Stellar Populations (SSPs) with three different ages from 0.1 to 1 Gyr, and the bottom panel shows a constant star formation rate model with fixed age of 0.1 Gyr and reddening from  $E_{B-V} = 0$  to 0.8. The templates shown are from the Maraston stellar population models (Maraston 2005). These models, however, are not supposed to be used for  $\lambda > 2.5 \mu\text{m}$  where they display a strong, unphysical, discontinuity. This discontinuity affects the IRAC colours at  $0 < z < 2.7$ . Hence we tested the reliability of this colour criterion also with BC03 templates, that are not affected by this problem. We verified that the expected IR colours for BC03 stellar population models at  $z < 2.7$  are equally bluer than the colour cuts defined by the equation 1.

From the upper panel of Fig. 5 it is clear that the 1.6  $\mu\text{m}$  peak criterion may lead to exclude some blue and unreddened ( $E_{B-V} = 0$ ) galaxy at  $z > 3.5$  with age  $< 0.1$  Gyr. This is because galaxies dominated by young stellar populations do not show the 1.6  $\mu\text{m}$  peak in their SEDs (see Sawicki 2002). In fact, due to this criterion we excluded from the final sample a spectroscopic confirmed LBG (object #5455, from Spinrad et al. 1998,

with  $z_{spec} = 5.34$  and  $z_{phot} = 5.18$ ), for which the best fit result predicted age  $\sim 7$  Myr, and mass  $\sim 10^{10} M_{\odot}$ . Nonetheless we decided to apply this criterion as a conservative way to obtain a reliable sample of the most massive galaxies at  $z \geq 3.5$ . The objects missed in this way are very few (see next section), and are also the least massive ones. Their inclusion would not strongly affect our estimate of the comoving stellar mass density (for more details see Sect. 5.2, 6.1 and 6.2).

**Table 2.** Sample selection criteria. In the left and right columns the subsequent steps to select the final sample and the corresponding number of objects are shown, respectively.

Selection Criteria	Number of Objects
$m_{4.5} \leq 23$	4142
$z_{phot} \geq 3.5$	140
No hard X-ray emission	125
IRAC/channel 4 peak	53

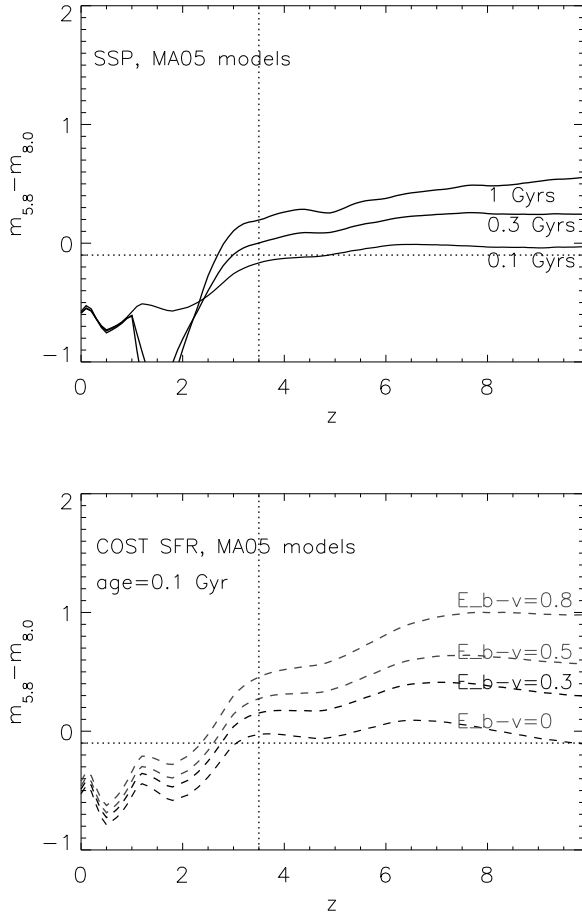


**Fig. 5.** The two panels show the  $m_{5.8} - m_{8.0}$  colour in function of redshift for the Maraston stellar population models (Maraston et al. 2006). Top panel: Single-burst Simple Stellar Populations (SSPs) with three different ages (0.1, 0.5 and 1 Gyr). Bottom panel: 0.1 Gyr stellar populations with constant star formation rate (SFR) and four different extinction values ( $E_{B-V} = 0.0, 0.3, 0.5, 0.8$ )

This criterion is very efficient in excluding SSPs galaxies with redshifts lower than  $\sim 2.5$ . On the other hand, we should point out that it cannot completely remove the contamination by interlopers at  $2.5 < z < 3.5$ , as SSPs models with ages  $> 1$  Gyr and  $3 < z < 3.5$ , and dusty star forming galaxies at  $2.5 < z < 3.5$  can still satisfy this criterion (see the bottom panel of the same figure).

Finally it should be noted that the adopted colour criterion would be met also by the so-called ‘IRAC power-law sources’. These objects are generally selected by requiring a rising SED over the four IRAC bands, and they are believed to be generally  $z < 2.5$  AGNs with a hot dust component swamping the stellar emission (Alonso-Herrero et al. 2006; Donley et al. 2007). Since Donley et al. (2007) selected a sample of (62) IRAC power-law galaxies in the Chandra Deep Field Nord (CDFN), whose 27 are in the GOODS-N field, we investigate the overlap with their sample. We found 10 sources in our  $4.5 \mu\text{m}$  IRAC-selected ( $m_{4.5} \leq 23$ ) sample (of 4142 objects) in common with the ‘IRAC power-law’ sample. All these sources but one have the infrared part of the SED peaked at  $8.0 \mu\text{m}$ , but most of them had been excluded from our  $z \geq 3.5$  final sample because of their lower photometric redshifts. Only one object of the Donley et al. (2007) sample fulfill all of our selection criteria. This is object #14793 in our sample (see Tab. 4 and Fig.14), corresponding to the object CDFN:[DRP2007]19080 in Donley et al. This galaxy has no X-ray emission ( $< 4.41 \times 10^{-16} \text{erg s}^{-1} \text{cm}^{-2}$ ) and a rather high  $24 \mu\text{m}$  flux ( $111 \pm 3.5 \mu\text{Jy}$ ). The high redshift solution is still consistent with these properties.

As result we obtained a final sample of 53 galaxies ( $\sim 43\%$  of the pre-selected  $z \geq 3.5$  sample), that we consider to be valid candidates at  $z \geq 3.5$ . About the 12% of the 125 pre-selected high- $z$  candidates have been discarded due to the low S/N ratio in the  $8.0 \mu\text{m}$ -band, but we cannot exclude that some of them could be at high redshift. The other 45% is likely mainly composed either by younger systems (age  $< 0.1$  Gyr) at the same redshift, or by lower redshift  $z < 3.5$  contaminants. We will show in the following that the former are only a minority (see Sect. 5.2). In Table 6, the multi-band photometry of the final sample is shown.

As a further test on the quality of this sample we checked how many candidates satisfy the empirical blending criterion tested on extensive simulations by the GOODS team and used by Daddi et al. (2007) and Dickinson et al. (2008 in prep.). This is based on the measurements of the angular separation ( $\Delta\theta$ ) between IRAC positions and the  $K$ -band counterparts (we used also optical coordinates for  $K$ -undetected sources). According this criterion, if a galaxy has  $\Delta\theta > 0''.5$ , it is likely contaminated by blending in the IRAC bands. However we should point out that this criterion proved to be successful on objects detected at the  $5\text{-}10\sigma$  in both of the  $K$  and IRAC bands. For sources with fainter optical and near-IR detections the shift of the centroid position throughout the different bands could be larger due to higher noise. Hence a larger  $\Delta\theta$  could derive from coordinate fluctuations rather than from blending contamination. Moreover due to the extremely red colours of our candidate high- $z$  galaxies, this criterion is not extensively applicable to our full sample being half of it both optical and near-IR undetected. Out of the sources with at least a reliable optical or near-IR detection ( $>3\text{-}5\sigma$ ) we verified that the majority (18/25) did pass this criterion. On the other hand we found 7 galaxies (#1098, #2172, #2796, #13857, #15268, #15541, #15761) with  $\Delta\theta > 0''.5$ . However for these objects the lack of visual evidence of blending led us to conclude that the quite large  $\Delta\theta$  separation, is a S/N issue. Moreover for two of these galaxies the confirmed spectro-



scopic redshifts (#13857, #15541, see Sect. 5.4) prove that the measured IRAC photometry leads to reliable SED fitting results.

### 5.1. Comparison between the BC03, MA05 models

The SED fitting analysis with BC03 and MA05 templates gives somewhat discordant results for both galaxy masses and ages estimate. This is an issue recently debated by several authors (e.g. Maraston et al. 2006; Kannappan & Gawiser 2007; Bruzual A 2007), the major source of this discrepancy being the different treatment of the Thermally Pulsing Asymptotic Giant Branch (TP-AGB) phase of stellar evolution in the population models.

In the MA05 models stars in the TP-AGB phase contribute a dominant source of bolometric and near-infrared light for stellar populations in the age range 0.2 to 2 Gyr, much larger than is found in the BC03 models. For those models the TP-AGB phase has been calibrated with local stellar populations. Another difference is in the treatment of convective overshooting. In their work Maraston et al. (2006) tested both the BC03 and MA05 models on a sample of high- $z$  galaxies, with reliable spectroscopic redshifts ( $1.4 \lesssim z \lesssim 2.5$ ) in the Hubble Ultra Deep Field (HUDF). They found that the results of MA05 models imply younger ages by a factors up to 6 and lower stellar masses, by 60% on average, with respect to BC03 (and in general to the others models of population synthesis). The overestimate of BC03 galaxy stellar masses, produced by the lack of the TP-AGB contribution to the integrated luminosity, become considerable for evolved stellar populations with ages between 0.5 and 2 Gyr.

In Fig. 6 we compare the stellar masses estimated for the  $z \geq 3.5$  galaxies with the two different template libraries (BC03 vs MA05). It appears that the BC03 models tend to overestimate galaxy masses of our sample with respect to the MA05 ones, by 0.15 dex on average (see the smaller panel on the top of Fig. 6), in good agreement with the previous studies (e.g. Maraston et al. 2006; Wuyts et al. 2007; Cimatti et al. 2008; Werner et al. 2004). In the rest of this paper we will adopt the MA05 stellar templates to compute the galaxy stellar masses and the comoving stellar mass density. However, in some cases we also use the BC03 models results for comparisons with the literature.

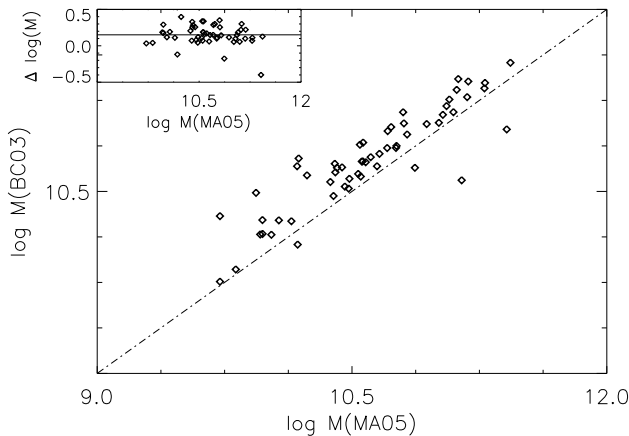


**Fig. 6.** Comparison between estimated masses by means of different template libraries for our final sample of 53 objects:  $\log M(\text{BC03})$  vs  $\log M(\text{MA05})$ . It is visible that BC03 models tend to overestimate galaxy masses with respect to the MA05 ones. The inserted panel shows the distribution of the  $\log M(\text{BC03}) - \log M(\text{MA05})$  relation as a function of the galaxy mass.

### 5.2. Comparison with Lyman break selection techniques

One of the most popular method used to identify high- $z$  galaxies is the ‘dropout’ technique, a colour selection based on the redshifted 912 Å Lyman-break caused by neutral hydrogen in the galaxy SEDs. This technique was introduced by Guhathakurta et al. (1990) and Steidel & Hamilton (1992) to select Lyman Break Galaxies (LBG) at  $z \approx 3$  (u-band dropout). It has been largely used also to identify galaxies in the redshift range  $z \sim 4 - 6$ , as b-, v- or i-dropout (Steidel et al. 1999; Dickinson 1998; Steidel et al. 2003; Giavalisco et al. 2004b). However this colour criterion is strongly biased against red massive galaxies at high redshift, that are faint or totally undetected in optical and near-IR bands.

To obtain a quantitative estimate of the fraction of red objects missed by combining optical magnitude limited selection and dropout techniques, we matched our final sample of IRAC-selected high redshift galaxies (53 objects) with a sample of  $B$ - and  $V$ -dropout LBGs in the GOODS-N field from Giavalisco et al. (2004a). We found that only 7 of our massive high- $z$  candidates are included in the  $B$ -dropout sample, and none in the  $V$ -dropout sample. This means that the remaining IR bright ( $m_{4.5} < 23$ )  $z \geq 3.5$  candidates have been missed by those selection criteria, due to their faint emission at optical and near-IR wavelengths (most of them having  $z_{850} > 27$ ).

While the vast majority of our candidates are missed by the dropout selection technique, there could also be a significant population of massive galaxies with  $m_{4.5} < 23$  that are identified through the dropout technique and that have been missed by our selection criteria. We tested for the presence of such galaxies using again the sample of Giavalisco et al. (2004a).

Giavalisco et al. (2004a) listed 684 LBGs candidates ( $B$ -dropout +  $V$ -dropout). Only 7 of those are also part of our sample of  $z > 3.5$  candidates. Only 32 of the Giavalisco et al. galaxies have  $m_{4.5} < 23$  (15  $B$ -dropout and 17  $V$ -dropout). Of these, 20 were excluded from our sample because of their photometric redshifts  $z < 3.5$  (8  $B$ -dropout and 12  $V$ -dropout). One more object ( $V$ -dropout) was excluded because of the presence of X-ray emission and 4 objects ( $V$ -dropouts) were excluded because of the lack of an IRAC-8.0  $\mu\text{m}$  peak. One of these 4  $V$ -dropout galaxies has a confirmed spectroscopic redshift of  $z = 5.2$  (see also Sect. 5). It is reasonable to suppose that all the 4  $V$ -dropouts galaxies that we excluded are actually genuine  $z > 3.5$  galaxies with young ages, lacking a distinct peak in the IRAC-8.0  $\mu\text{m}$  band. Even taking them into account would increase our sample of  $z > 3.5$  galaxy candidates by only 7% and would reduce to 81% the fraction of  $z > 3.5$  massive galaxies that are lost by the UV dropout selection techniques.

It is also interesting to make a comparison with the Lyman-break galaxies samples selected by Eyles et al. (2007) and Stark et al. (2007) in the GOODS-South field. The former work reports 6 galaxies at  $z \sim 6$  with masses in the range  $1 - 2.4 \times 10^{10} M_{\odot}$ , and 4.5  $\mu\text{m}$  magnitude  $m_{4.5} > 23$ . Since the authors used Salpeter IMF and BC03 models to derive galaxy SEDs, we have to consider that galaxy masses for these 6 objects are overestimated by a factor of  $\sim 2.4$  ( $2.4 = 1.4 \times 1.7$ , being 1.4 and 1.7 the conversion factors from BC03 to MA05 and from Salpeter to Chabrier IMF, respectively Pozzetti et al. 2007; Cimatti et al. 2008, see also Sect. 5.1 and Sect. 6.2). When rescaled, masses span the range  $0.4 - 1 \times 10^{10} M_{\odot}$ , with only one galaxy with  $M \sim 10^{10} M_{\odot}$ . Lyman Break Galaxies similar to the ones found by Eyles et al. (2007) would not be included in our sample, since these are fainter than our magnitude cut  $m_{4.5} = 23$ . This issue is

in agreement with the lower masses found for these LBGs with respect to our high- $z$  sample.

The latter work also reports 6 galaxies, spectroscopically confirmed at  $z \sim 4.4 - 5.6$ . We used the same conversion factor to rescale galaxy masses from BC03 and Salpeter IMF and we found that only three galaxies of the Stark et al. (2007) sample have masses  $> 10^{10} M_{\odot}$ . Moreover only two out of these three sources have  $m_{4.5} < 23$ .

Hence only 4 galaxies out of the 12 LBGs at  $4.4 \leq z \leq 6$  from the two works, fall within our mass bracket ( $M \sim 10^{10} - 10^{11} M_{\odot}$ ), and only two would meet our magnitude selection ( $m_{4.5} < 23$ ). The two IRAC brightest and most massive sources from Stark et al. (2007) have ages  $\sim 150$  Myr, if rescaled by a factor of 6 to account for the overestimate produced by BC03 models (Maraston et al. 2006), and  $E_{B-V} \sim 0.0$ . We can suppose that they are similar to the youngest unreddened population excluded from our final sample by the  $8 \mu\text{m}$  peak criterion (see Sect. 5 and Fig. 5, top panel), such as the 4 V-band dropout galaxies of the sample of Giavalisco et al. (2004b). The other two galaxies with masses  $\sim 10^{10} M_{\odot}$  and fainter than our IRAC magnitude selection would be even younger (ages  $< 100$  Myr).

In conclusion, it seems that we are not missing a significant population of sources with our selection criteria. A few blue star forming galaxies with young ages are indeed excluded but these objects have generally low stellar masses that would not meet our stellar mass completeness limits ( $M_{\star} \geq 5 \times 10^{10} M_{\odot}$ ; see Sect. 6.1 and 6.2).

### 5.3. $24 \mu\text{m}$ emission

We used observations at  $24 \mu\text{m}$  with *Spitzer* +MIPS to give some constraints on the ‘‘activity’’ of our high redshift galaxy candidates. Detection of  $24 \mu\text{m}$  flux for  $z > 3.5$  galaxy candidates could be explained in terms of radiation coming from star formation activity lately re-processed and re-emitted by the dust (emission lines from PAH molecules), or with the presence of an highly obscured AGN in relatively quiescent galaxies. We divided our sample of high redshift candidates in two sub-samples: MIPS-detected (MIPS-d) and MIPS-undetected (MIPS-u) samples and discuss them separately in the following.

#### 5.3.1. The MIPS-u sample

21 objects in our sample are undetected in MIPS down to the limit of  $20 \mu\text{Jy}$ . The best fit Spectral Energy Distributions (SEDs) of the MIPS-u sub-sample is presented on the left panels of Fig. 13. The right panels of the same figure show the  $\chi^2_{\nu}$  distribution as a function of redshift for each of the sources. We also report the most probable photometric redshift solution ( $z_{\text{phot}}$ ). The best fitting parameters and the estimated galaxy masses are presented in Table 3. Most of the MIPS-u redshifts are spread around a median value of  $z \sim 4$ , in a redshift range  $z=3.5-5$ . We find that the best fitting SEDs give  $\chi^2_{\nu} < 2$  for 20 out of 21 objects and no degeneracy on the redshift solution for the majority of the sources. On the contrary, we find also lower redshift solutions within the 90% confidence intervals of  $\chi^2_{\nu}$  distribution for 5 objects (# 4008, # 9561, # 12327 and #14130), caused mainly by the redshift-reddening degeneracy (see Tab. 3 and Fig. 13).

To further constraints on the nature of the stellar populations of MIPS-u galaxies we compared their  $z - m_{4.5}$  colours with the expected ones for MA05 SSP models with different ages (0.1, 0.3 and 0.5 Gyr). The results are shown in Fig. 7. Although the MIPS-u objects span a large range of  $z - m_{4.5}$  colours, most of

them show colours consistent with older starlight (0.3–0.5 Gyr). On the contrary, a smaller part of the sub-sample (7 objects) shows bluer colours, more compatible with younger SSPs (0.1–0.3 Gyr), probably implying ongoing star formation activity.

The SED fitting analysis and the lack of mid-IR  $24 \mu\text{m}$  emission could thus suggest that many of the MIPS-u galaxies might be ‘quiescent’, non dusty candidates at  $z \geq 3.5$ . However, we should not forget that the MIPS observations in the field are not deep enough to unequivocally constrain the lack of star formation in these galaxies. The  $24 \mu\text{m}$  emission is generally used as SFR indicator in high-redshift galaxies ( $z \sim 2$  to 3; Daddi et al. 2005; Papovich et al. 2007; Yan et al. 2007; Rigby et al. 2008). Following Chary & Elbaz (2001) we can estimate that a source at  $z \sim 4$  with a  $24 \mu\text{m}$  flux of  $20 \mu\text{Jy}$  will have a total IR luminosity of  $\sim 1.5 \times 10^{13} L_{\odot}$ , corresponding to a SFR of  $\sim 1500 M_{\odot} \text{yr}^{-1}$  for a Chabrier IMF (Kennicutt 1998). Therefore the  $24 \mu\text{m}$  non-detection imposes only a very loose upper limit to the SFR. However, the  $24 \mu\text{m}$  non-detection is a necessary condition for quiescent systems (given the MIPS flux limit). In the following analysis we will use the MIPS-u galaxy sample to derive an upper limit to the space density and stellar mass density of ‘quiescent’ candidates at  $z \sim 4$  (Sect. 6.3).

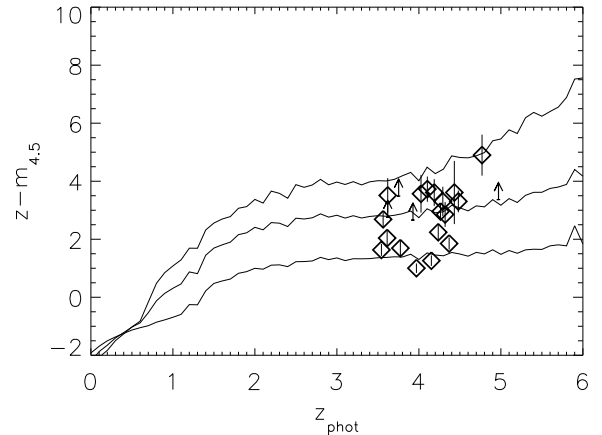


**Fig. 7.** Comparison between the observed  $z - m_{4.5}$  colours of the MIPS-u galaxies (black open diamonds) and the ones predicted at the same redshift for SSPs models (MA05) with different ages (black curves in the figure, with age of 0.1, 0.3 and 0.5 Gyr, respectively, from the lower part upward). Most MIPS-u objects have  $z - m_{4.5}$  colours consistent with SSPs with ages in the range of 0.3–0.5 Gyr. On the contrary, a smaller part of the sub-sample (7 objects) shows bluer colors, more compatible with younger SSPs (0.1–0.3 Gyr), probably exhibiting star formation activity.

#### 5.3.2. The MIPS-d sample

Out of the 53 galaxies of our high- $z$  sample, more than half (32) are detected at  $24 \mu\text{m}$ . The best fitting SED results for the MIPS-d objects and their relative  $\chi^2_{\nu}$  distributions within the 90% confidence intervals are shown in Fig. 14. In Table 4 we report the best fitting parameters for the MIPS-d sample. The quality of the fit for the MIPS-d SEDs is very good, with  $\chi^2_{\nu}$  values below 1.5 for almost all objects (except for #5511, which has  $\chi^2_{\nu} = 2.46$ ). However most galaxies in the sub-sample present degenerate redshift solutions, caused by the different models used and the amount of reddening present (# 702, # 2560, # 2796,

#ID	$z_{phot}$	$\chi_v^2$	$P_{\chi_v^2}$	$A_V$	$z_{inf-90\%}$	$z_{sup-90\%}$	$z_{2-phot}$	$P_{\chi_{v,2}^2}$	log M(MA05)
#522	3.928	0.410	94.28	0.80	3.060	5.230	10.060	43.52	9.960
#1098	4.369	1.465	14.55	0.20	4.250	4.460	4.922	0.04	10.143
#2574	3.620	0.307	97.98	0.40	2.570	4.110	6.098	0.47	10.581
#3081	3.543	0.466	91.26	0.70	3.340	3.760	0.456	0.00	9.816
#3302	4.292	0.306	98.01	0.30	3.620	4.600	10.060	0.00	10.565
#4008	9.024	0.201	99.63	0.40	2.150	10.060	3.753	99.57	10.069 <sup>a</sup>
#5073	4.481	0.738	68.90	0.20	4.250	4.670	3.417	20.62	11.073
#5460	4.236	0.854	57.65	0.00	3.480	4.390	3.683	50.87	10.402
#6876	3.620	0.683	74.09	0.20	2.220	4.040	3.172	72.67	10.485
#7042	3.774	0.646	77.54	0.50	3.340	3.900	3.529	75.10	9.723
#7286	3.564	5.582	0.00	0.10	2.850	3.620	3.193	0.00	10.610
#7309	3.613	1.267	24.30	0.00	3.130	3.830	3.417	22.90	9.723
#7785	3.970	1.964	3.28	0.30	3.900	4.040	0.540	0.00	10.391
#8403	4.264	2.018	2.76	0.00	4.110	4.390	3.347	0.57	10.710
#9537	4.103	0.150	99.89	0.40	3.200	4.390	6.651	0.00	10.801
#9561	4.026	0.838	59.14	0.00	2.080	4.320	3.396	51.28	10.412
#11682	4.320	0.367	96.11	0.00	4.040	4.530	2.941	64.89	10.186
#12327	4.971	0.202	99.41	0.70	2.920	7.750	3.256	96.17	11.185
#14130	4.432	0.315	97.06	0.10	1.590	5.090	3.067	96.30	10.235
#14260	4.152	1.243	25.71	0.50	4.040	4.250	0.652	0.01	9.935
#15268	4.775	2.534	0.47	0.80	4.390	5.090	7.260	0.07	10.373

**Table 3.** Best fitting parameters for the MIPS-u sample. In the order: identification number,  $z$  (best fit solution),  $\chi_v^2$ , probability relative to  $z$ , reddening, upper and lower bound for the 90% confidence interval,  $z_{2-phot}$  (second best solution), probability relative to  $z_{2-phot}$ . We should point out that, for galaxies with  $z_{phot} \sim 8 - 10$ , the best fit redshifts result uncertain, and the equally probable solution range ( $z_{inf} - z_{sup}$ ), within the 90% of confidence, is very large. Also for some of these objects -marked by the footnote<sup>a</sup>- the *hyperzmass* procedure was not able to find any physical solution by fitting the data points with MA05 models the extreme redshifts.

<sup>a</sup> This value for the galaxy mass was found for the secondary solution of photometric redshift,  $z = 3.753$ , because the *hyperzmass* software did not find a plausible solution at  $z = 9.024$ .

# 3393, # 3850, # 5157, # 5367, # 6099, # 9301, # 9306, # 10176, # 11304, # 13129, # 14105).

It is difficult to understand the nature of these objects, given that often high and lower photometric redshift solutions result equally probable. In these cases the  $24 \mu\text{m}$  emission could be interpreted in different ways, depending on the redshift of the objects and on the reddening parameter. Assuming that  $z \geq 3.5$  is correct, and taking into account the lack of hard-X ray emission, the MIPS flux could ensue from highly obscured AGNs hosted in relatively quiescent galaxies. However, still consistently with the high redshift solution, the  $24 \mu\text{m}$  emission could be also due to star formation at extreme high rates. In the next section we will examine this possibility using sub-mm/mm photometry from the SCUBA ‘supermap’ (Borys et al. 2003; Pope et al. 2005), and the MAMBO (Greve et al. 2008) and AzTEC (Perera et al. 2008) imaging surveys of GOODS-N.

On the other hand if the lower redshift solution ( $z \sim 2 - 3$ ) is considered, the  $24 \mu\text{m}$  emission could be explained in terms of PAH emission from dust heated by star formation activity, and those objects would be accounted as dusty star-burst galaxies at  $z \sim 2 - 3$ .

#### 5.4. Sub-mm detections : a large population of massive starburst galaxies at $z \sim 4$ ?

Sub-mm/mm selected galaxies (hereafter SMGs) are the brightest star forming galaxies known, being much more more luminous than the local ultra-luminous IR galaxies -ULIRGs- with  $L_{IR} \gg 10^{12} L_{\odot}$ . These galaxies are massive young objects seen during their formation epochs, with very high SFR (Lilly et al. 1999; Scott et al. 2002), about one order of magnitude larger than that of typical systems with similar masses (Daddi et al. 2007). They are also fairly rare objects, probably due to the short du-

ration of their bright phase ( $\ll 100 \text{ Myr}$ ; Greve et al. 2005). These objects could represent the common early phase in the formation of massive elliptical galaxies, and hence they might be crucial link to understand the massive galaxy formation process.

The numerous sub-mm datasets available in the GOODS-N field can be used to improve the constraints on the nature of our  $z \geq 3.5$  candidates.

We made direct comparison with three sub-mm maps of the field:

- the Sub-millimeter Common User Bolometer Array (SCUBA, Holland et al. 1999) ‘supermap’ of 35 SMGs selected with  $S/N \geq 4$  at  $850 \mu\text{m}$  (Borys et al. 2003; Pope et al. 2005, 2006);
- the Max Planck Millimeter Bolometer Array (MAMBO, IRAM 30-m telescope, Bertoldi et al. 2000)  $1200 \mu\text{m}$  map from Greve et al. (2008), composed by 27 sources detected with  $3.5 \leq S/N < 4$  and 20 with  $S/N \geq 4$ ;
- the AzTEC (Wilson et al. 2008, ,15 m James Clerk Maxwell Telescope -JCMT)  $1100 \mu\text{m}$  map of 28 sources detected with  $S/N \leq 3.75$  (Perera et al. 2008).

We used a simple approach, looking for overlap of our sample with the position of the submm/mm selected galaxies in the above works. We have used radial separation limits of  $7''$ ,  $6''$  and  $9''$ , to search for matches with galaxies in the SCUBA, MAMBO and AzTEC, respectively.

We found eight of our high- $z$  candidates in the error box of the SCUBA ‘supermap’ sources (#5157, #6099, #6463, #8520, #10176, #11682, #13857, #15541), but only seven (except #11682) correspond to the IRAC counterparts identified by Pope et al. (2006). For two of these galaxies, GN20 and GN20.2, (objects #15541, #13857 in our sample) spectroscopic redshifts

ID	$z_{phot}$	$\chi^2_V$	$P_{\chi^2}$	$A_V$	$z_{inf-90\%}$	$z_{sup-90\%}$	$z_{2-phot}$	$P_{\chi^2,2}$	$\log M(\text{MA05})$
# 588	4.285	0.785	64.36	0.60	3.690	4.740	9.388	0.05	9.973
# 702	8.814	0.067	99.99	0.40	1.450	10.060	3.340	99.99	10.563
#1720	3.522	0.526	87.33	0.60	2.850	4.250	3.921	84.30	10.399
#2172	3.711	0.536	86.56	0.70	3.550	4.180	4.117	70.42	11.097
#2560	3.830	0.044	100.00	0.40	2.780	8.520	7.274	100.00	10.762
#2796	10.060	0.279	98.59	0.80	3.360	10.060	3.536	95.36	10.870 <sup>a</sup>
#2894	3.893	0.628	79.14	0.70	2.990	4.460	10.060	0.37	10.441
#3393	5.503	0.477	90.59	0.80	3.830	5.860	5.167	84.73	10.647
#3850	4.166	0.063	100.00	0.70	3.410	9.290	8.009	99.90	10.940
#5157	4.740	0.344	96.90	0.00	4.110	7.400	6.504	92.59	11.433
#5367	4.355	0.494	89.51	0.80	3.900	4.880	10.060	0.03	10.806
#5511	4.152	2.521	0.50	0.50	4.040	4.250	1.310	0.00	10.551
#6099	5.251	0.367	96.10	0.10	3.200	8.450	4.999	96.02	11.178
#6245	5.062	0.108	99.98	0.00	4.460	5.370	2.934	81.31	10.662
#6463	9.437	0.193	99.68	0.10	3.690	10.060	4.215	99.64	9.973 <sup>a</sup>
#8520	3.683	0.573	83.71	0.00	3.340	3.830	3.137	44.99	10.730
#9007	3.669	1.117	34.42	0.60	2.780	4.110	2.969	34.41	10.824
#9301	8.226	0.059	100.00	0.20	2.640	10.060	8.037	100.00	11.035
#9306	8.660	0.127	99.95	0.80	2.360	10.060	8.219	99.92	11.011
#9782	3.928	1.472	14.28	0.20	3.480	4.320	8.723	0.02	11.116
#10176	5.818	0.002	100.00	0.20	3.550	9.570	5.517	100.00	11.280
#11304	4.145	0.378	95.67	0.80	3.550	8.100	5.461	89.78	10.759
#12699	3.543	1.760	6.21	0.30	3.200	3.690	3.354	5.62	10.558
#13129	7.960	0.030	100.00	0.20	3.410	10.060	8.296	100.00	11.056
#13857	3.746	0.863	56.74	0.10	3.270	4.040	3.403	43.23	10.707
#14505	3.564	0.014	100.00	0.80	2.920	10.060	7.757	100.00	10.025
#14668	4.600	0.209	99.56	0.10	1.870	5.230	4.789	99.53	10.177
#14722	4.145	1.816	5.23	0.40	4.110	4.180	0.617	0.36	10.180
#14793	4.474	1.225	27.41	0.00	4.040	5.160	9.185	0.01	11.411
#15541	3.949	1.216	27.45	0.40	3.690	4.110	0.680	0.00	11.146
#15761	4.292	0.177	99.78	0.10	3.900	4.530	6.567	0.00	11.126
#15771	3.564	0.360	96.35	0.20	3.060	3.830	6.854	0.00	11.283

**Table 4.** Best fitting parameters for the MIPS-d sample. In the order: identification number,  $z$  (best fit solution),  $\chi^2_V$ , probability relative to  $z$ , reddening, upper and lower bound for the 90% confidence interval,  $z_{2-phot}$  (second best solution), probability relative to  $z_{2-phot}$ . For the objects with extremely high redshift best fit solutions, the same caveat we gave in Tab. 3 should be taken into account

<sup>a</sup> These values for the galaxy masses were found for the secondary solutions of photometric redshift, because the *hyperzmass* software did not find a acceptable solution at  $z \sim 9 - 10$ .

around  $z \sim 4$  were recently determined by Daddi et al. (2008, hereafter D08). Those objects are among the most distant SMGs spectroscopically confirmed known at the present. Our photometric redshifts for these galaxies are consistent within the error ( $\sim 0.2$ ) with the spectroscopic ones (being 3.75 and 3.95 for GN20 and GN20.2 respectively). It is interesting to remark that D08 discuss the evidence of a galaxy proto-cluster at  $z \sim 4$  in the GN20 and GN20.2 area, due to the finding of an over-density of B-dropout galaxies. Four objects in total from our  $z > 3.5$  sample (#13857, #14722, #15268, #15541) are also within a 25'' radius centered on the coordinates of GN20. This represents an over-density of a factor of 18 with respect to the expected number density of IRAC-selected galaxies in the field. Massive galaxies seem to be tracing this proto-cluster structure at  $z = 4.05$ .

We found five sources of our high- $z$  sample matching the MAMBO galaxies within the correlation distance. Out of them only #15541 (GN20) is also SCUBA-detected. In addition, 8 objects from the AzTEC survey correspond to galaxies in our  $z > 3.5$  sample, within the adopted search radius. Three of them are also SCUBA detected, and three are in common with the MAMBO survey from G08.

Candidate  $z > 3.5$  galaxies in our sample that are consistent with being counterpart of SCUBA, MAMBO and/or AzTEC sources are listed in Tab. 5.

It should be noted that the bulk of the sub-mm counterparts, except the objects #522 (GN1200.5/AzGN06) and #7785 (GN1200.46), are 24  $\mu\text{m}$ -detected (MIPS-d sample). The latter is also a less secure MAMBO detection, being among the sources with a S/N below the 4.5  $\sigma$  limit, and is not part of the ‘robust deboosted catalogue’.

We can check the reliability of the high- $z$  solution for the sub-mm detections by comparing their  $S_{850}/S_{24}$  vs  $S_{24}/S_{8.0}$  colours with the ones found by D08 for the two confirmed SMGs galaxies at redshift  $\sim 4$  (GN20 and GN20.2). We show this comparison in Fig. 8, where GN20 and GN20.2a are represented as black bold diamonds. As suggested by D08, starburst galaxies at  $z \sim 4$  would have relatively blue Spitzer MIPS-IRAC colours, similarly to GN20 and GN20.2a ( $\log(S_{24}/S_{8.0}) < 0.7$ ,  $\log(S_{24}/S_{4.5}) < 1.11$ ). Moreover, because of the negative sub-mm k-correction the  $S_{850}/S_{24}$  ratio should increase with redshift. Hence we expect that starburst at  $z \sim 4$  would occupy the upper-left part of the diagram in Fig. 8, with  $\log(S_{850}/S_{24}) > 2$  (such as GN20 and GN20.2a).

ID (this paper)	SCUBA name	MAMBO/AzTEC name	$z_{phot}$ (this paper)	$z_{min90\%}$	$z_{max90\%}$	$z_{phot}$ (P06)	$z_{radio-IR}$ (D08)	$S_{850}$ [mJy]	$S_{1200/1100}$ [mJy]	d [arcsec]
#588	...	.../AzGN12	4.28	3.69	4.74	...	...	...	3.07	5.2
#3850	...	.../AzGN20N	4.17	3.41	9.29	...	...	...	2.79	2.3
#5367	...	.../AzGN27N	4.35	3.90	4.88	...	...	...	2.31	6.5
#14505	...	GN1200.9/AzGN28	3.56	2.92	10.06	...	...	...	2.7/2.31	4.1/4.2
#522	...	GN1200.5/AzGN06	3.93	3.06	5.23	...	...	...	3.8/4.13	2.9/1.1
#7785	...	GN1200.46/...	3.97	3.90	4.04	...	...	...	2.1 <sup>a</sup>	4.5
#11304	...	GN1200.13/...	4.14	3.55	8.10	...	...	...	2.2	0.8
#6099	GN03	...	5.25	2.95	10.0	2.0	1.9	1.8	...	2.5
#10176	GN09	.../AzGN31	5.818	3.55	10.0	2.4	13.42	8.9	2.13	3.9/5.3
#5157	GN11	...	4.74	4.11	7.40	2.3	2.45	7.0	...	2.4
#8520	GN12	.../AzGN08	3.68	3.34	3.83	3.1	3.20	8.6	3.83	5.16/8.7
#6463	GN18	...	9.437/4.215	3.7	10.0	2.2	2.50	3.2	...	3.2
#15541	GN20	GN1200.1/AzGN01	3.949	3.69	4.11	2.95	<b>4.055</b>	20.3	9.3/10.69	1.3/1.9/1.4
#13857	GN20.2a	...	3.746	3.27	4.04	2.83	<b>4.051</b>	9.9	...	6.2

**Table 5.** SCUBA, MAMBO and AzTEC counterparts found in our  $z \geq 3.5$  of MIPS-d detected sources. In the columns we report: the ID number of the objects (this paper); the names from the sub-mm surveys; photometric redshift estimated in this paper and their 90% confidence intervals; photometric redshifts by Pope et al. (2006, P06); radio-IR redshifts by Daddi et al. (2008, D08) - with the two spectroscopic values in boldface-; the SCUBA, MAMBO and AzTEC fluxes. The last column is the distances between the proposed IRAC-4.5  $\mu\text{m}$  counterparts and the sub-mm positions.

<sup>a</sup> Not deboosted flux

Out of the SCUBA sources (black diamonds), two (#10176/GN09 and #8520/GN12) have mid-IR colours comparable with GN20 and GN20.2a, and  $\log(S_{850}/S_{24}) > 2$ . This finding can be seen as a further confirmation of the  $z > 3.5$  redshift estimated for these objects. It is also in agreement, within the 99% confidence interval, with the radio-IR redshifts estimated by D08 (see their Tab. 3). In the same figure also the ‘SCUBA-blank’ MAMBO (red triangles) and AzTEC (green crosses) detections are shown. To represent them in this diagram we scaled the  $S_{1200}$  and  $S_{1100}$  fluxes to  $S_{850}$ , multiplying by a factor of 2, i.e. the typical  $S_{850}/S_{1200}$  ratio found for GN20 and GN20.2 (D08). This is also consistent with the  $S_{850}/S_{1100}$  flux ratio derived by Perera et al. (2008,  $2.08 \pm 0.18$ ). For the MIPS-u #522 and #7785 we show the limits in the two-colours diagram, computed with  $S_{24}=20 \mu\text{Jy}$  (the  $5 \sigma$  24  $\mu\text{m}$ -MIPS flux lower limit). Also the sub-mm-IR colours of these sources are consistent, within the error bars, with the expected colours for high- $z$  SMGs. For comparison we show also the positions occupied in Fig 8 by the other sub-mm galaxies from the (Pope et al. 2006) sample with secure IRAC counterparts, that do not overlap with our sample. Almost all these sources (violet small squares) are spectroscopically confirmed at  $z \sim 1 - 2.5$  (see Pope et al. 2006). The evidence that most of them occupy the lower-right part of Fig 8 strongly support the above statements. Other two galaxies from the SCUBA ‘supermap’ have colours similar to GN20 and GN20.2, i.e. GN10, and GN22. The first one is claimed by several authors (D08, Dannerbauer et al. 2008; Wang et al. 2007, 2009) to be a  $z > 3.7$  starburst, although (Pope et al. 2006) report a  $z = 2.2$  photometric redshift. The second one is a spectroscopically confirmed galaxy at  $z = 2.509$  (Chapman et al. 2005; Pope et al. 2006). It represents the only case in the SCUBA sample of a lower-redshift sub-mm/mm emitter with both  $S_{850}/S_{24}$  ratio and IRAC colours similar to spectroscopic confirmed  $z \geq 3.5$  SMGs. Nevertheless from a statistical point of view the diagram shown in Fig 8 seems to be a valid diagnostic to prove high- $z$  starburst for sub-mm/mm sources.

Hence we can conclude that, for  $\sim 78\%$  of the galaxies in our sample that are likely sub-mm/mm detected, these results support the hypothesis of extreme SFR activity at high- $z$ .

Instead the sub-mm (SCUBA) sources lying in the right part of Fig. 8 (objects #5157, #6099 and #6463  $\sim 22\%$  of the sub-mm detections) are more probably at lower redshifts, as proposed by Pope et al. (2006).

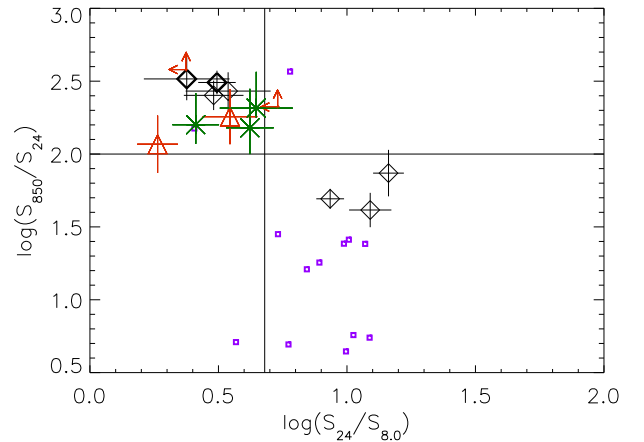


**Fig. 8.**  $S_{850}/S_{24}$  vs  $S_{24}/S_{8.0}$  colours for the SCUBA (black diamonds), MAMBO (red triangles) and AzTEC (green crosses) detections of our high- $z$  sample. The comparison with the GN20 and GN20.2 (Daddi et al. 2008) seems to support the high- $z$  hypothesis for most of these sources (left part of the diagram; see Sect.5.4). The solid black line represent the colour limit suggested by (Daddi et al. 2008) for sub-mm galaxies at  $z \geq 4$  ( $\log(S_{24}/S_{8.0}) < 0.7$ ). The small violet squares are the SCUBA ‘supermap’ sources that do not overlap with our high- $z$  sample, most of them spectroscopically confirmed at  $z \sim 1 - 2.5$ .

### 5.5. Mid-IR vs IR colours

The properties and the overall spectral energy distributions make the MIPS-d galaxies comparable to one of the most debated objects in the literature, HUDF-JD2. This object, identified as

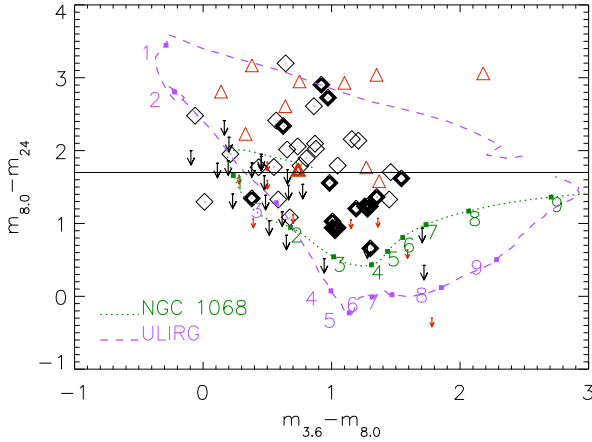


**Fig. 9.** Infrared colours  $m_{8.0} - m_{24}$  vs  $m_{3.6} - m_{8.0}$  of our high- $z$  sample of galaxies (black diamonds) compared with the objects found by Rodighiero et al. (2007) (red open triangles). The bold red triangle represents HUDF-JD2 (Mobasher et al. 2005). Bold black open diamonds are the SCUBA detected galaxies of our sample. The two objects with confirmed  $z \sim 4$ , GN20 and GN20.2, are highlighted (filled black diamonds). The MIPS-undetected objects are shown as upper limits in the  $m_{8.0} - m_{24}$  colour: black and red arrows for our sample and Rodighiero et al. (2007) sample, respectively. Two evolutionary colour tracks of an ULIRG (violet dot-dashed curve; Chary & Elbaz 2001), and of a galaxy hosting an obscured AGN (dashed green curve; Seyfert 2 galaxy NGC 1068), with increasing redshift values, are also shown. The black horizontal line represents the upper limit suggested by D08 and also shown in Fig. 8 for colours of starburst galaxies at  $z \geq 3.5$ .

a  $z \sim 3.4$  galaxy by Yan et al. (2004) and Chen & Marzke (2004), was recently suggested by Mobasher et al. (2005) as a massive post star-burst galaxy at  $z \approx 6.5$  hosting an obscured AGN. However subsequent studies (Dunlop et al. 2007; Rodighiero et al. 2007; Chary et al. 2007) claimed that HUDF-JD2 is more likely a lower redshift ( $z \sim 1.5-2.2$ ) star forming galaxy with very strong dust reddening. Our galaxies are also similar to candidate  $z > 4$  galaxies found by Rodighiero et al. (2007) and Wiklind et al. (2008). In Fig. 9, the infrared colours ( $m_{8.0} - m_{24}$  vs  $m_{3.6} - m_{8.0}$ ) of our high- $z$  sample (open black diamonds) are compared with the objects found by Rodighiero et al. (2007, open red triangles). The bold red triangle represents HUDF-JD2 (Mobasher et al. 2005). Bold black open diamonds are the sub-mm detected galaxies of our high- $z$  sample. The two objects with confirmed  $z \sim 4$ , GN20 and GN20.2, are represented by filled black diamonds. The MIPS-undetected objects are shown as upper limits in the  $m_{8.0} - m_{24}$  colour (black and red arrows for our sample and the sample of Rodighiero et al. 2007, respectively). The evolutionary colour tracks of an ULIRG (Chary & Elbaz 2001) and of a galaxy hosting an obscured AGN (the Seyfert 2 galaxy NGC 1068) with increasing redshift values are also shown. It is clear, though, that such locally calibrated templates are not very useful to interpret the colors of distant galaxies. This can be argued just considering that the observed  $m_{8.0} - m_{24}$  colours of GN20 and GN20.2 are  $\sim 1$  mag redder with respect to the ULIRG track at  $z \sim 4$ . As discussed in Daddi et al. (2008), this is most likely due to a lower stellar mass to light ratio in the distant galaxies.

The black horizontal line represents the upper limit suggested by D08 and also shown in Fig. 8 for colours of starburst galaxies at  $z \geq 3.5$  ( $\log(S_{24}/S_{8.0}) < 0.7$ , in AB magnitude:  $m_{8.0} - m_{24} < 1.7$ ; see also Sect. 5.4). If the high- $z$  solution is

correct, objects bluer than this limit should be strongly dominated by star formation, such as GN20 and GN20.2. The issue that most of the the sub-mm detected galaxies in our sample are down to the black line in the figure also suggest that they have properties similar to the two starbursts spectroscopically confirmed at  $z \sim 4$ . The MIPS-d sources which have similar colours but are lacking in a sub-mm counterpart could be also high- $z$  starbursts. Alternatively, the lack of sub-mm detection should be justified either by the shallow sensitivity of the currently available sub-mm instruments (SCUBA, MAMBO, AzTEC), or by particularly “warm” SEDs for this objects.

On the other hand, the  $z \geq 3.5$  candidates with  $m_{8.0} - m_{24} > 1.7$  in Fig. 9 could represent a different population. Their redder colours, more similar to the bulk of the Rodighiero et al. (2007) sample, could be due to heavily obscured AGN, as also suggested by Rodighiero et al. (2007) for most of their sources, or they might be  $z < 3.5$  contaminants. The position of object HUDF-JD2, overlapping with the solid black line in the middle part of the diagram, does not allow us to give any further constraint on its nature.

## 6. The comoving stellar mass density at $3.5 < z < 5$

Recent studies (Drory et al. 2005; Fontana et al. 2006; Stark et al. 2007; Verma et al. 2007; Eyles et al. 2007; Yan et al. 2006) have extended measurements of the total stellar mass density up to  $z \sim 4 - 5$ , using deep multicolour data from optical and near-IR selected samples. One of the goals of this paper is to determine how our IRAC-4.5 selected sample contributes to the comoving stellar mass density at  $z \geq 3.5$ . In fact, as already discussed, observations of the high redshift Universe are generally biased against red galaxies with large mass-to-light ratios, potentially missing galaxies that could potentially make a strong contribution to the total mass density (see Fontana et al. 2006). Here, we emphasize that we can only determine a lower limit to the comoving stellar mass density in the redshift interval  $3.5 \leq z \leq 5$ , for several reasons. First, the combination of our IRAC  $4.5 \mu\text{m}$  magnitude limit and the  $1.6 \mu\text{m}$  peak SED criterion leads to missing objects with lower masses at these redshifts, such as the fainter, bluer Lyman break galaxies, as we have discussed in Sect. 5. More generally, a magnitude-limited sample (selected at any wavelength) is not the same as a mass-limited sample, as we will discuss further in the next section.

### 6.1. Incompleteness effects and mass selection criteria

In estimating the comoving stellar mass density we must take into account that our sample could suffer from incompleteness. As several other authors (Fontana et al. 2004; Drory et al. 2004; Labbé et al. 2005) have noted, IR-selected samples are still not equivalent to mass-selected samples. In fact, at any redshift, the galaxies detected above the sample magnitude limit can have a fairly large range of possible  $M_{\star}/L$  ratios, depending on their spectral properties, ages, dust extinction, metallicities, etc. The effect is that magnitude-limited samples, at higher redshifts, are progressively biased against objects with lower masses and high  $M_{\star}/L$  ratios, such as galaxies that are not currently forming stars, or which are highly extinguished.

We have attempted to evaluate the consequences and minimize the effects of incompleteness by determining the threshold mass limit as a function of redshift for a variety of galaxy models spanning a range of ages and degrees of extinction. For this purpose we used the MA05 template library with the Chabrier IMF, the same as was used in the preceding sections to derive

the galaxy stellar masses. We consider both the simplest case of SSP models with different ages (0.1, 0.5 and 1 Gyr), and a set of models with a constant star formation rate, an age of 0.5 Gyr, and different amounts of extinction ( $E_{B-V} = 0.0, 0.3, 0.5$ , applied using the Calzetti attenuation law; Calzetti et al. 2000). The observed  $4.5 \mu\text{m}$  flux as a function of redshift was derived from these models, and from this we translate our  $4.5 \mu\text{m}$  magnitude limit ( $m_{4.5} \leq 23$ ) into a limiting stellar mass at each redshift. The results are shown in Fig. 10. For passively evolving galaxies (i.e., the SSPs) with ages less than 0.5 Gyr, and for star-forming galaxies with  $E_{B-V} < 0.3$ , our sample should be fairly complete at  $M > 5 \times 10^{10} M_{\odot}$  out to  $z < 5$ . This is another advantage of our  $4.5 \mu\text{m}$  sample selection from the very deep GOODS IRAC data, which is complete to significantly lower mass thresholds at these very high redshifts compared to  $K$ -selected samples (see Fontana et al. 2006).

Assuming that the redshift estimate for the objects in our high- $z$  sample are correct, we derive their contribution to the comoving number density and to the total stellar mass density, both for the total sample (MIPS-u+MIPS-d) and for the MIPS-u sample only, in the redshift interval  $3.5 \leq z \leq 5$  as described in the following sections. The comoving volume in this redshift range over the total GOODS-N solid angle ( $\sim 165 \text{ arcmin}^2$ , coincident with the ACS  $z$ -band area) is  $V_{\text{com}} \sim 0.725 \times 10^6 \text{ Mpc}^3$ .

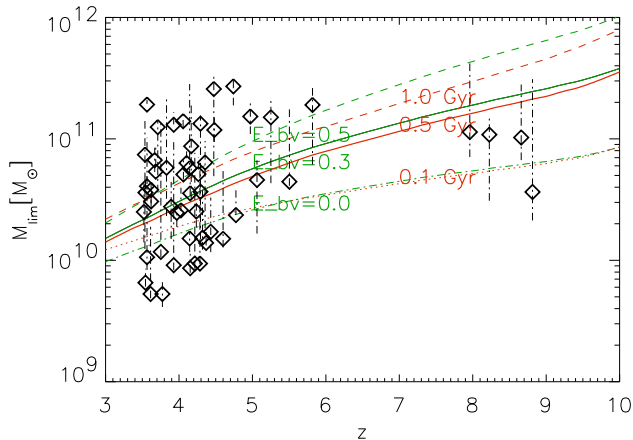


**Fig. 10.** The redshift dependence of the stellar mass limit for our IRAC magnitude-limited sample ( $m_{4.5} \leq 23$ ), derived from MA05 stellar population synthesis models. The red curves represent SSP models with different ages (0.1, 0.5 and 1 Gyr). The green curves are models with constant SFR, an age of 0.5 Gyr, and dust extinction, with three different values of the colour excess  $E_{B-V}$  (0.0, 0.3 and 0.5). The points indicate the objects of our  $z \geq 3.5$  sample, with error bars indicating the 68% confidence ranges on their stellar masses.

### 6.2. Contribution to the stellar mass density from our total sample in the redshift bin $z = 3.5 - 5$

Based on the preceding analysis, we assume a limiting stellar mass  $M \sim 5 \times 10^{10} M_{\odot}$  as the completeness threshold for our magnitude-limited sample. For quiescent galaxies with intermediate ages ( $\sim 0.5$  Gyr), we should be complete above this mass threshold out to  $z \sim 5$ . However, for  $z > 4$ , we may be incomplete near this mass limit for the oldest possible passive stellar populations, or for heavily dust-obscured galaxies.

Given this potential incompleteness, and the fact that we are undoubtedly missing a large percentage of bluer, lower-mass LBGs in the same redshift range (as discussed in section 5.2), we must consider our estimate for the stellar mass density at  $3.5 \leq z \leq 5$  to be a lower limit. Fig. 10 shows the derived stellar masses versus redshift for the objects in our IRAC-selected sample. We count objects and sum their stellar masses for galaxies above our mass threshold ( $M \sim 5 \times 10^{10} M_{\odot}$ ). The resulting comoving number density and the stellar mass density for this sample are  $2.6 \times 10^{-5} \text{ Mpc}^{-3}$  and  $(2.9 \pm 1.5) \times 10^6 M_{\odot} \text{ Mpc}^{-3}$ , respectively.

In Fig. 11 we show our lower limit to the comoving stellar mass density ( $\rho_*$ ) at  $3.5 < z < 5$ , and compare it to another estimate (Fontana et al. 2006, F06) at  $3 < z < 4$  for galaxies in a similar mass range ( $M_{\star} = 3 \times 10^{10} - 3 \times 10^{11} M_{\odot}$ ). We take the F06 value from the compilation published by Wilkins et al. (2008), and have corrected it for the  $M/L$  differences between the Salpeter and Chabrier IMFs ( $\log M(\text{Chabrier}) = \log M(\text{Salpeter}) - 0.23$ ), as well as by a factor of 1.4 to account for the difference between the BC03 used by F06 and the MA05 models used in our study (Sect. 5.1). We also show a curve derived from the Millennium Simulation models for the redshift evolution of the stellar mass density, computed for galaxy masses above the threshold limit of  $\geq 5 \times 10^{10} M_{\odot}$ . Assuming that the photometric redshifts for all the selected high- $z$  candidates are correct, our results are in good agreement with the Millennium Simulation predictions.

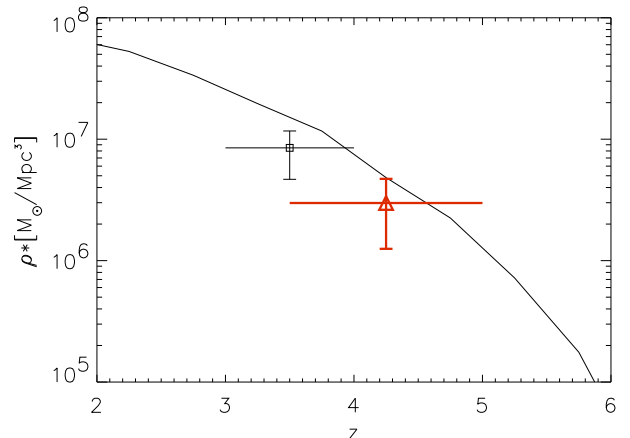


**Fig. 11.** Comparison between our estimate of the lower limit of the stellar mass density ( $\rho_*$ ) at  $3.5 < z < 5$  (red triangle) and the stellar mass density estimated by Fontana et al. (2006, F06) at  $3 < z < 4$ , for galaxies in the mass range  $M_{\star} \sim 3 \times 10^{10} - 3 \times 10^{11} M_{\odot}$ . The curve shows the evolution of stellar mass density with redshift from the Millennium Simulation models, computed for galaxies above our threshold limit of  $\geq 5 \times 10^{10} M_{\odot}$ .

### 6.3. Stellar mass density for the MIPS-u candidates in the redshift bin $z = 3.5 - 5$

As described above, our sample should be largely complete for ‘quiescent’, non-star-forming galaxies with ages  $\leq 0.5$  Gyr and masses  $M > 5 \times 10^{10} M_{\odot}$ . However, at these large redshifts, the flux limit at  $24 \mu\text{m}$ , even for very deep data from GOODS, corresponds to quite large star formation rates  $> 1000 M_{\odot}/\text{yr}$ . Therefore, we cannot affirm that the MIPS-undetected (MIPS-

u) objects in are sample are truly ‘quiescent’, and thus we can only derive an upper limit for the number and stellar mass densities of quiescent galaxies. For the MIPS-u subsample with stellar masses  $\geq 5 \times 10^{10} M_{\odot}$  at  $z = 3.5 - 5$ , we find a comoving number density of  $0.97 \times 10^{-5} \text{ Mpc}^{-3}$ , and a stellar mass density of  $(1.15 \pm 0.7) \times 10^6 M_{\odot} \text{ Mpc}^{-3}$  (MA05 templates and Chabrier IMF).

In Fig. 12 we compare our results for the MIPS-u sample with estimates of the stellar mass density for quiescent galaxies at other redshifts from the literature. To facilitate this comparison, here we have scaled all values to the Chabrier IMF and MA05 models by means of the  $M/L$  conversion relations given above (see Sect.6.2). We have also computed the comoving stellar mass density of the MIPS-u galaxies considering the unlikely case that they were all truly “passive”, consistent with single burst stellar populations (SSPs) with no dust. The masses were derived using the ratio between the observed IRAC-4.5  $\mu\text{m}$  flux for each galaxy and the expected flux for an MA05 SSP model at the same redshift, assuming an age of  $\sim 0.5$  Gyr and mass normalized to  $1 M_{\odot}$ . In this case, the number density of MIPS-u candidates above the mass threshold would be larger ( $1.52 \times 10^{-5} \text{ Mpc}^{-3}$ ). The corresponding stellar mass density would be  $(1.46 \pm 0.7) \times 10^6 M_{\odot} \text{ Mpc}^{-3}$ . This value is also represented in Fig. 12 by the red dashed line. From this exercise we concluded that even if all the MIPS-u galaxies were considered as old SSPs, the number density of ‘quiescent’ galaxies at  $z = 3.5 - 5$  would remain very small in comparison with that found at  $z \leq 2 - 2.5$  by previous studies.

The stellar mass density we found for the MIPS-u galaxies in the redshift range  $z = 3.5 - 5$  is  $\sim 2$  orders of magnitude lower than the local value (black asterisk; Baldry et al. 2004), and more than 10 times lower than the values found at  $z \sim 1.7$  by Daddi et al. (2005, ; black filled rhombus) for the passive-BzK galaxies in the Hubble Ultra Deep Field (HUDF) and at  $z \sim 2.5$  by Labbé et al. (2005, black open square) for Distant Red Galaxies (DRGs) in the Hubble Deep Field South. Moreover our result is also in good agreement with the mass density estimated by Wiklind et al. (2008) for  $z \sim 5.5$  Balmer-break-selected galaxies without MIPS detections in the GOODS South Field at redshift  $z \sim 5.5$  (open rhombus in the figure). Considering that our estimate is an upper limit to the comoving stellar mass density of massive and quiescent galaxies, we conclude that there is evidence of strong evolution beyond  $z \sim 2$  (see also Daddi et al. 2005). The decreasing number density of quiescent objects at high redshifts could mean that most massive galaxies at early epochs were experiencing strong star formation activity.

## 7. Summary and conclusions

In recent years, a substantial number of massive galaxies have been found at redshifts as large as  $z \sim 5$ . However, although the range of stellar populations and observed colors among galaxies at all redshifts studied to date has proven to be quite heterogeneous, most surveys at  $z > 3.5$  to date have primarily selected samples of star-forming blue galaxies, and have been biased against red massive objects that are faint or completely undetected in optical and near-IR bands.

In this work we have studied galaxies selected at IRAC-4.5  $\mu\text{m}$  in the GOODS-N field, in a manner that is complementary with respect to optical or near-IR selection. This allows us to pick out massive, evolved galaxies at high redshift, for which the optical rest frame emission (which is most nearly related to the stellar mass) is sampled by the redshifted, rest-frame near-

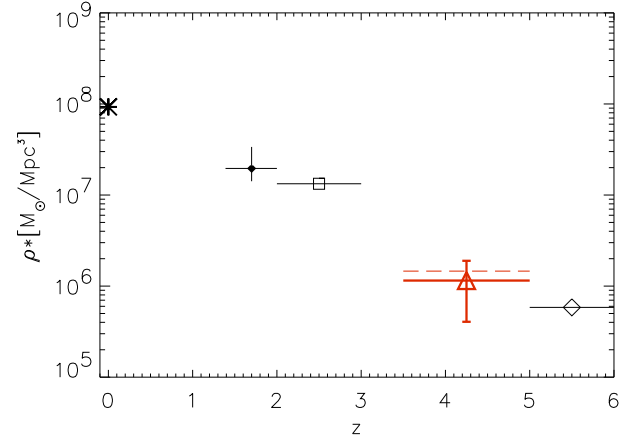


**Fig. 12.** Comparison between the upper limit to stellar mass density ( $\rho_*$ ) found in this paper for ‘quiescent’ galaxies in the redshift bin  $z = 3.5 - 5$  and results from the literature at other redshifts. All points have been scaled to Chabrier IMF and MA05 masses (see Sect. 6.2). Our estimate is represented as a red bold triangle. The horizontal red dashed line represent the stellar mass density we derive by considering all MIPS-u galaxies to be SSPs with age of 0.5 Gyr. The local mass density in passive galaxies is shown by the black asterisk (Baldry et al. 2004). The black open square is for Distant Red Galaxies (DRGs) at  $z = 2 - 3$  in the Hubble Deep Field South (Labbé et al. 2005). The black filled rhombus is from Daddi et al. (2005) for passive-BzK galaxies in the Hubble Ultra Deep Field (HUDF) at  $z = 1.39 - 2$ , and the open rhombus is for Balmer-break MIPS undetected galaxies at  $z = 5 - 7$  in GOODS-South from Wiklind et al. (2008).

infrared portion of the spectrum. On the other hand, this selection may also be sensitive to ‘active’ obscured galaxies at high redshift, for which IR emission could be reprocessed radiation from absorbing material surrounding an AGN, or from dust heated by star formation, like that seen in dusty starburst galaxies such as local ULIRGs.

Recently, other studies based on near-IR selection have detected red, massive galaxy candidates at  $z_{\text{phot}} \geq 4$ , but have not obtained complete samples. In most of these studies, the samples have been selected in the  $K$ -band, with the possibility of missing  $K$ -undetected objects visible in the longer-wavelength IRAC filters (e.g. Mobasher et al. 2005; Wiklind et al. 2008). Rodighiero et al. (2007) used IRAC-3.6  $\mu\text{m}$  selection ( $m_{3.6} < 23.26$ ) to identify a sample of high- $z$  galaxies missed by optical and  $K$ -band selection. However they assumed as additional conditions the non-detection of their candidates in optical bands, and a detection close to the sky threshold limit in the  $K$  band ( $K > 23$ , AB system), which make their sample *a priori* incomplete.

Here, we attempt to select a sample of massive high redshift red galaxies that is as complete as possible, by means of IRAC selection, that could allow us to recover massive objects that may have been missed by previous studies. The most important results of this paper are summarized in the following items:

- By selecting at IRAC-4.5  $\mu\text{m}$  ( $m_{4.5} \leq 23$ ), we extracted a sample of 4 142 objects in the  $\sim 165 \text{ arcmin}^2$  of the GOODS-N field. We performed an SED fitting analysis to estimate photometric redshifts for those objects, and found fifty-three candidates at  $z \geq 3.5$ , also requiring that peak of the  $f_{\nu}$  stellar spectral energy distribution (at  $1.6 \mu\text{m}$  in the rest-frame) falls in the IRAC-8.0  $\mu\text{m}$  band. We excluded unobscured AGN from our final sample, identified by their hard and/or soft-X ray emission. Almost 81% of our candidates are completely



missed by the  $B$ - and  $V$ -band Lyman break dropout techniques designed to identify UV-bright, star-forming galaxies at similar redshifts. For each object, we evaluate the reliability and the confidence limits of our photometric redshift estimates with a  $\chi^2$  test. Two objects have spectroscopically confirmed redshifts (GN20 and GN20.2; Daddi et al. 2008) in good agreement with our estimates.

- We divide our final sample in two sub-samples of (32) MIPS-detected and (21) MIPS-undetected objects (the MIPS-d and MIPS-u samples, respectively).

**MIPS-d sample:** In the subsample detected at  $24\mu\text{m}$ , we found 18 galaxies with unambiguous high photometric redshift solutions and 14 with degenerate solutions. If the high redshift solution is correct, the  $24\mu\text{m}$  emission could indicate the presence of a heavily obscured AGN (perhaps Compton thick due to the absence of X ray emission), or perhaps strong star formation activity in a dusty, hyperluminous starburst. We cannot firmly exclude the possibility for these galaxies to be dusty starburst galaxies at lower redshifts, for which the  $24\mu\text{m}$  flux could be explained with PAH emission at  $z \sim 2 - 3$ .

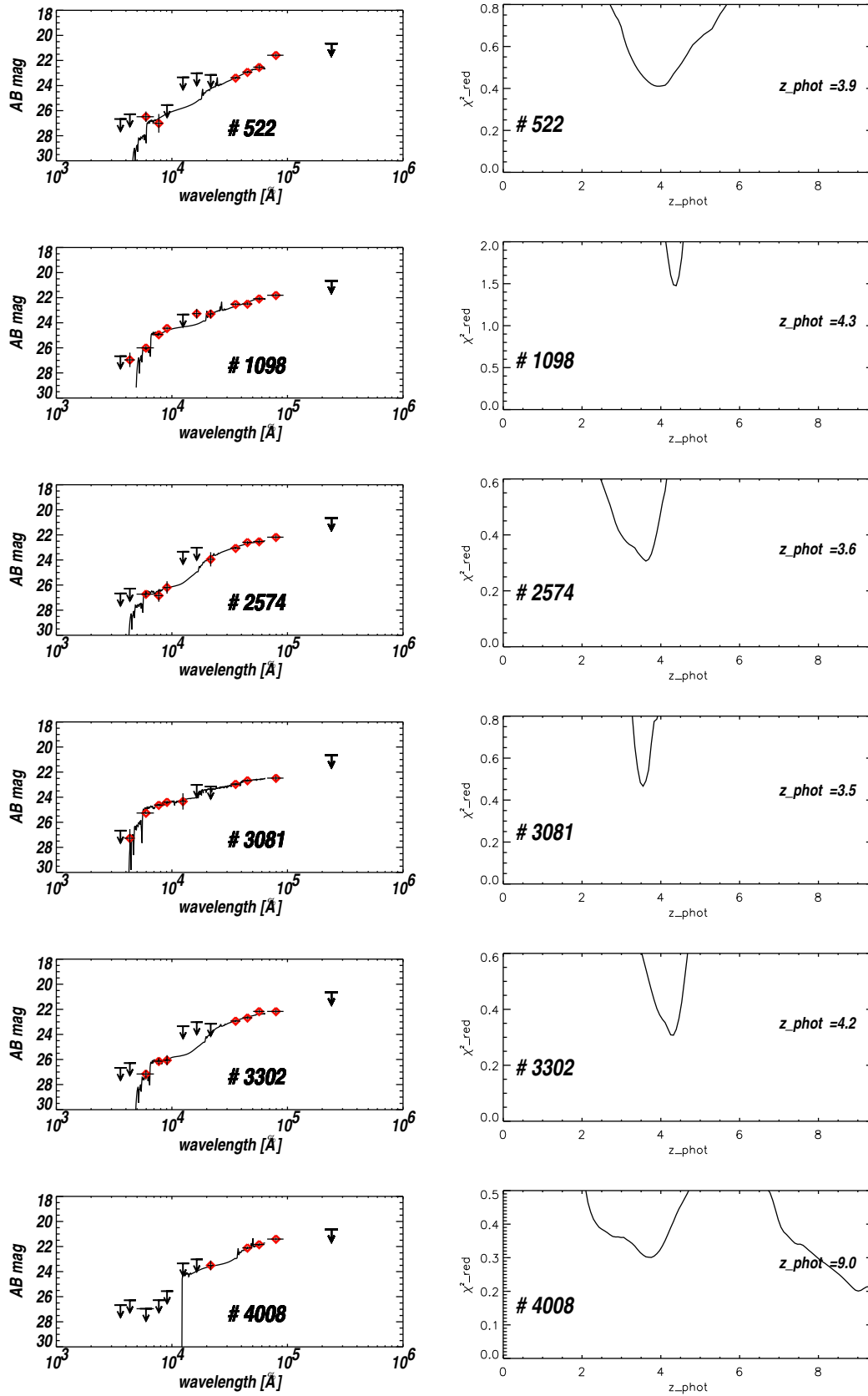
**MIPS-u sample:** 21 of our  $z \geq 3.5$  candidates are undetected at  $24\mu\text{m}$ . The lack of  $24\mu\text{m}$  emission is a necessary but not sufficient condition to indicate that these are quiescent galaxy. The upper limit to the SFR set by MIPS detection limit ( $f_{24} < 20\mu\text{Jy}$ ) corresponds to a star formation rate  $< 1500 M_{\odot}\text{yr}^{-1}$ , assuming bolometric corrections derived from spectral templates for local ultraluminous infrared galaxies. For this reason we can use this sub-sample only to give an upper limit to the total stellar mass of ‘quiescent’ galaxies at  $z \geq 3.5$ .

- 14 galaxies from our  $z \geq 3.5$  sample are detected at submillimeter and millimeter wavelengths with SCUBA (Pope et al. 2006), MAMBO (Greve et al. 2008) and AzTEC (Perera et al. 2008). All but two of are also detected at  $24\mu\text{m}$ . Two objects, GN20 and GN20.2, have spectroscopically confirmed redshifts at  $z \sim 4$  Daddi et al. (2008). By comparing their colours with other SMGs galaxies in the  $S_{850}/S_{24}$  vs  $S_{24}/S_8$  diagram, we find that  $\sim 78\%$  of the sub-mm detected objects among our candidates have properties that are fully consistent with those of starburst galaxies at  $z \geq 3.5$ . The remaining  $\sim 22\%$  are more likely at lower redshift.
- We have computed the contribution to the number density and to the stellar mass density by the total (MIPS-d+MIPS-u) sample and by the subsample that is undetected at  $24\mu\text{m}$  (MIPS-u) for galaxies with stellar masses above a limit of  $5 \times 10^{10} M_{\odot}$ , chosen to minimize incompleteness at  $z < 5$ . For the redshift range  $3.5 < z < 5$ , we find a comoving number density  $2.6 \times 10^{-5} \text{Mpc}^{-3}$  for average masses of  $\sim 10^{11} M_{\odot}$ . The corresponding stellar mass density is  $(2.9 \pm 1.5) \times 10^6 M_{\odot}\text{Mpc}^{-3}$ . Our results are in good agreement with previous determinations in the literature, and with the prediction from the Millennium simulations.

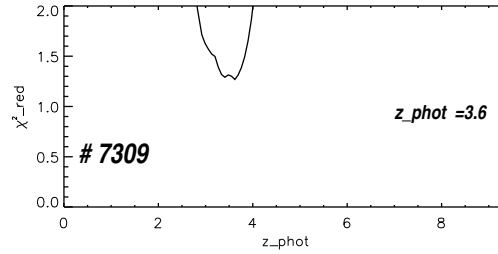
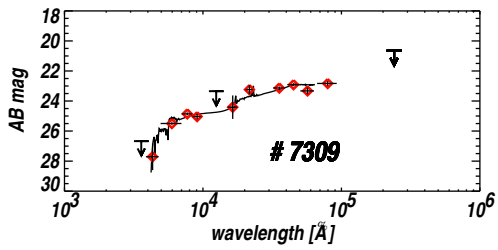
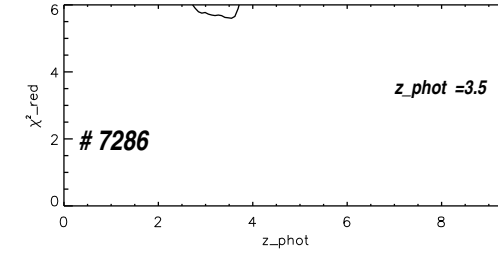
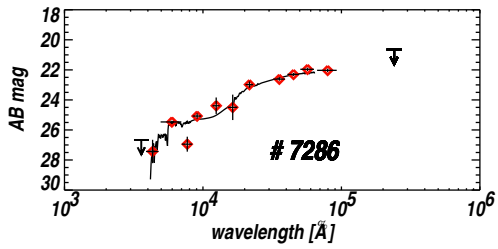
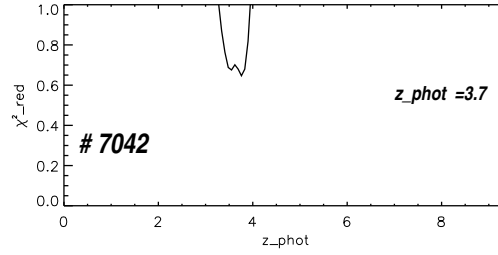
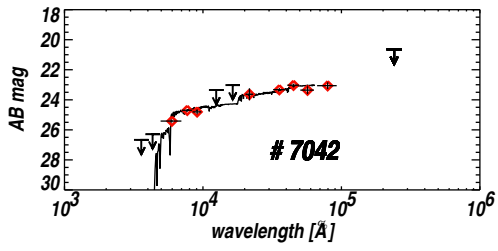
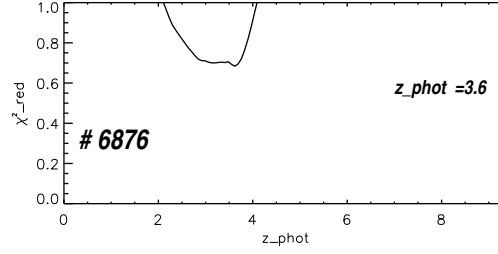
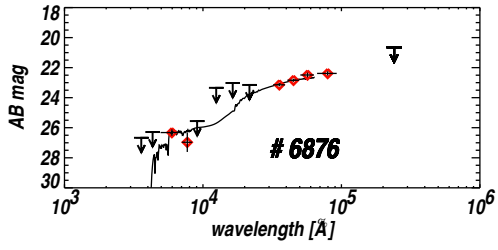
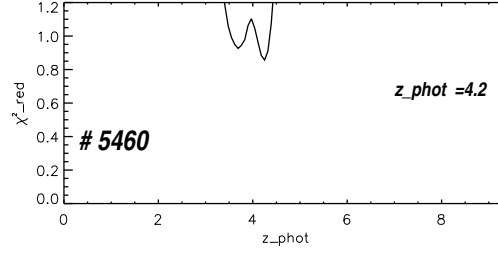
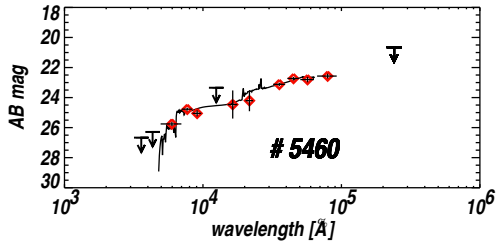
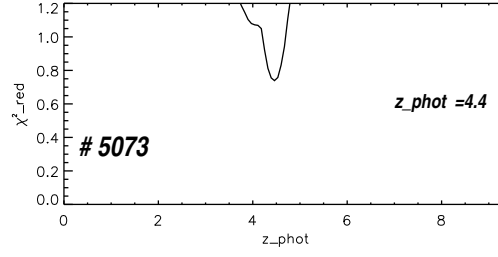
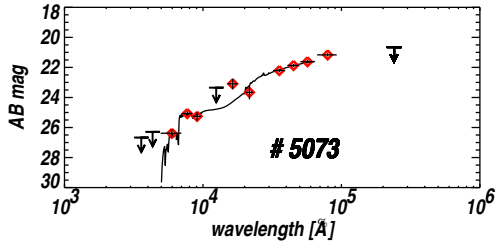
For the MIPS-u sample, we determined a number density of  $0.97 \times 10^{-5} \text{Mpc}^{-3}$  and a corresponding stellar mass density of  $(1.15 \pm 0.7) \times 10^6 M_{\odot}\text{Mpc}^{-3}$ . We also considered the extreme case that all of the MIPS-undetected galaxies were purely quiescent, with ages  $\sim 0.5$  Gyr. This results in larger upper limits for their number and stellar mass densities,  $1.52 \times 10^{-5} \text{Mpc}^{-3}$  and  $(1.46 \pm 0.7) \times 10^6 M_{\odot}\text{Mpc}^{-3}$  respectively. Our MIPS-u sample of quiescent candidates accounts for  $\sim 5 - 6\%$  of the mass density that was in place at  $z \sim 2$  and only for  $\sim 1\%$  of local stellar mass density (Baldry et al. 2004). This provides evidence for strong growth in the

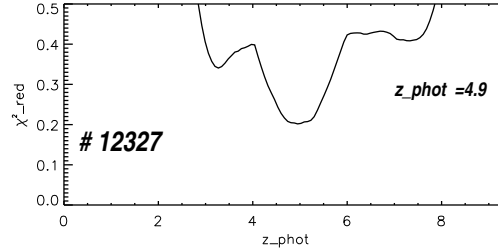
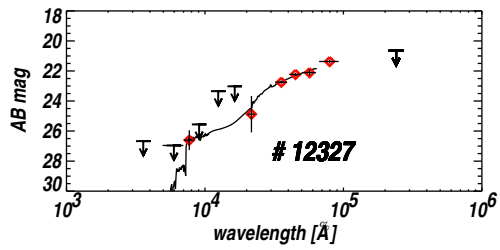
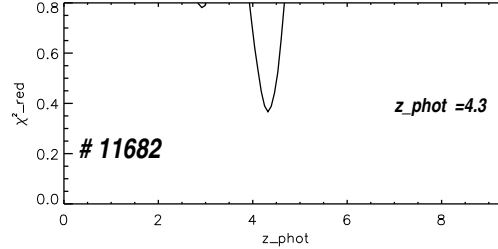
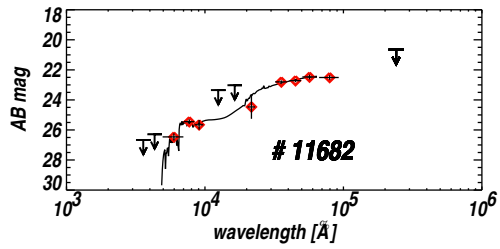
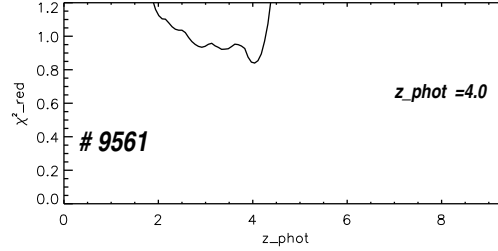
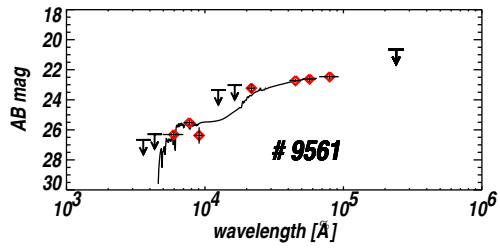
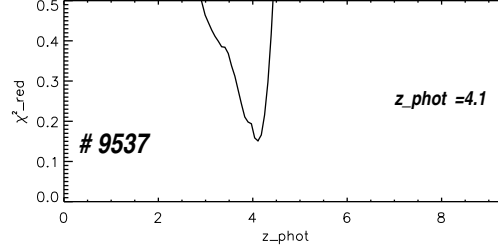
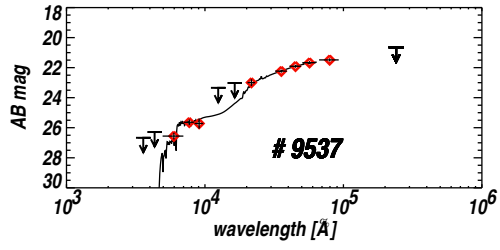
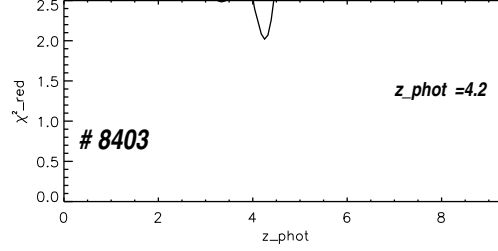
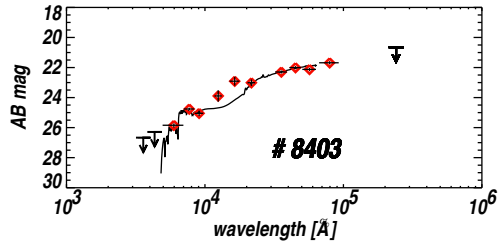
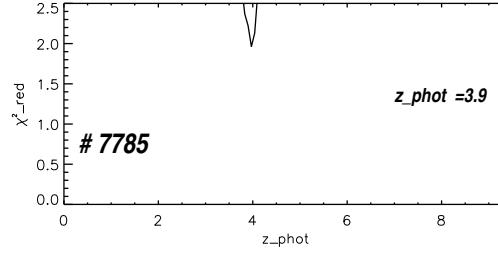
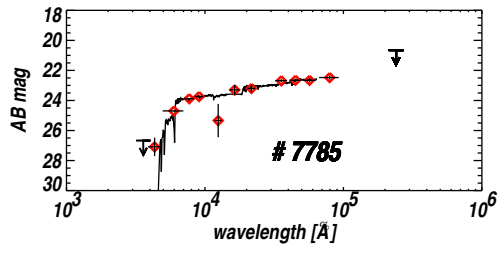
number of massive galaxies between redshift  $z = 4 - 5$  and  $z = 2$ .

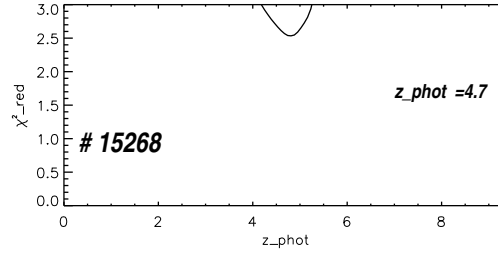
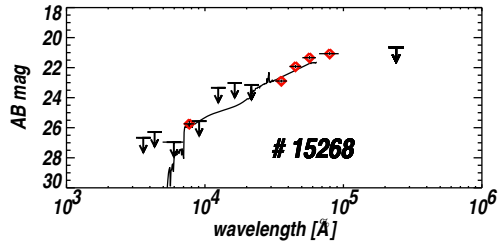
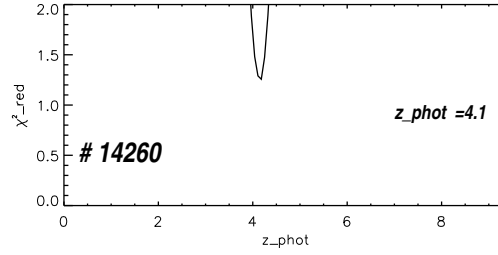
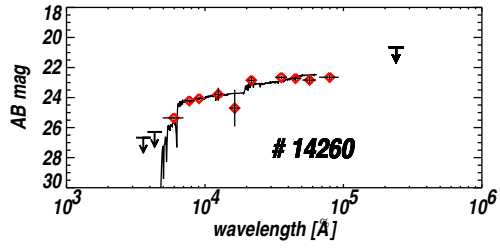
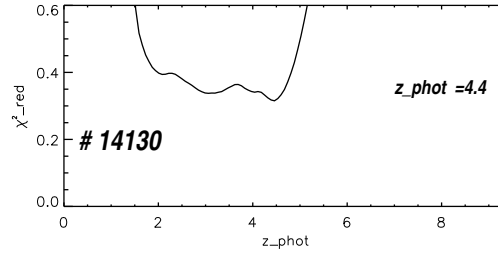
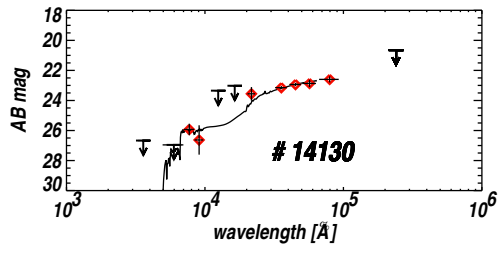
*Acknowledgements.* We thank Kyoung-Soo Lee for her reductions of the KPNO-4m FLAMINGOS imaging data of the GOODS-North field, and for information about the details of this data set. CM and ED acknowledge support from the French ANR grant numbers ANR-07-BLAN-0228 and ANR-08-JCJC-0008.

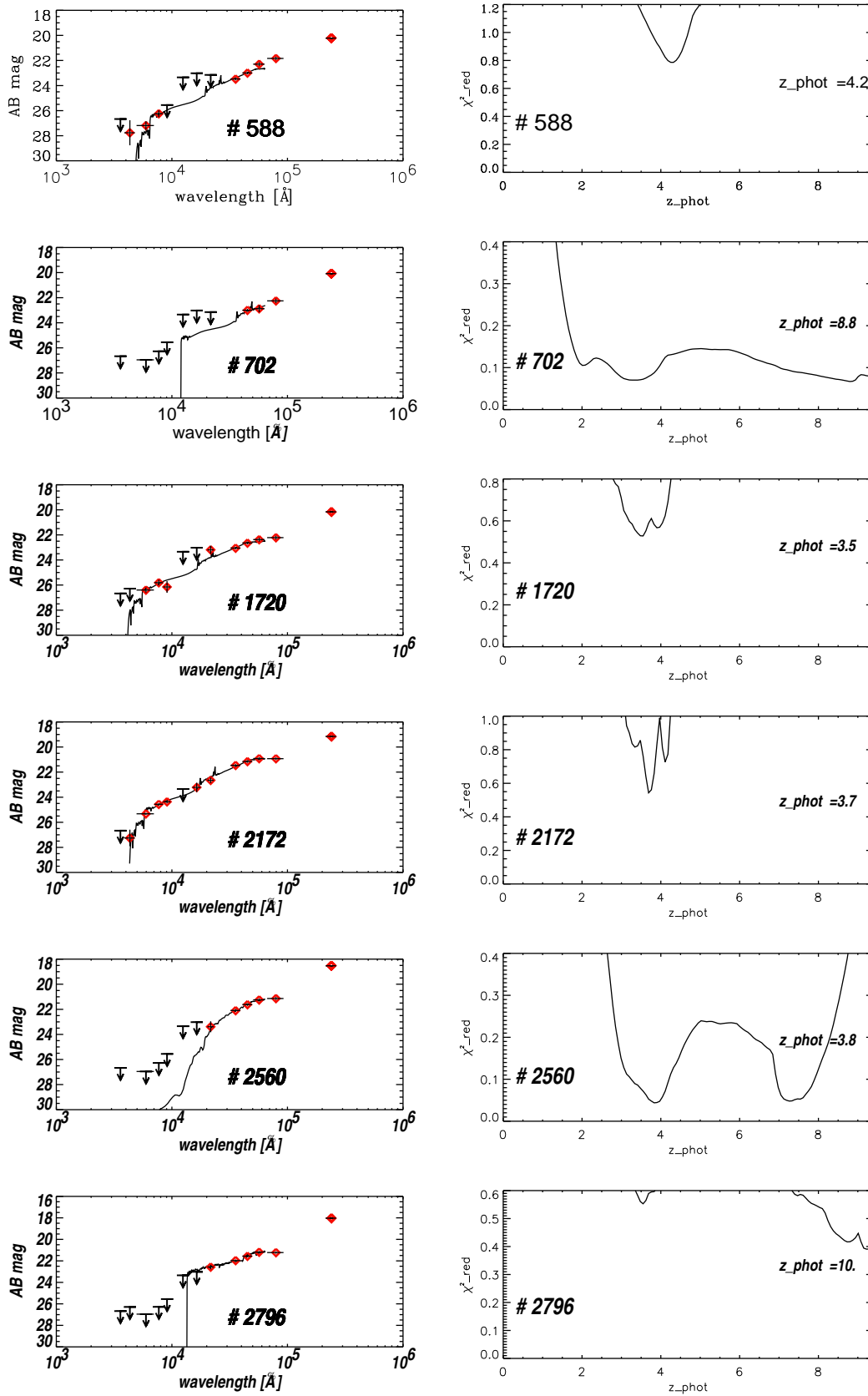


**Fig. 13.** Spectral Energy Distribution best-fit models for the MIPS-u sample in units of AB magnitude. The red diamonds represent the observed magnitudes from the photometric data. Non-detections are represented by upper limits. See also Tab. 3.

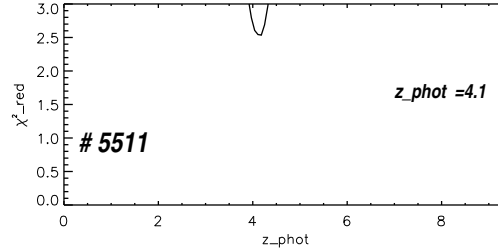
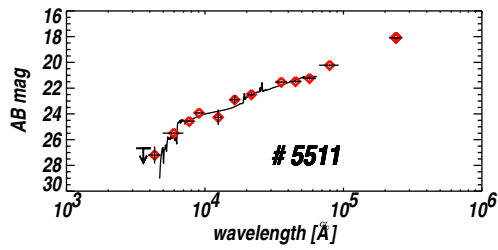
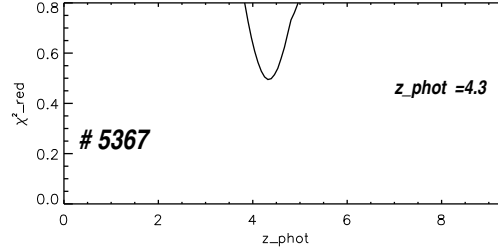
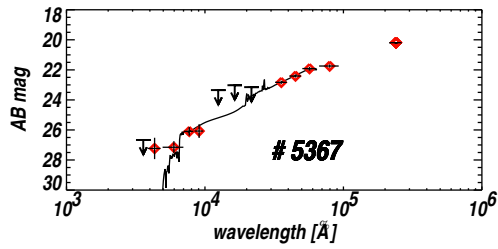
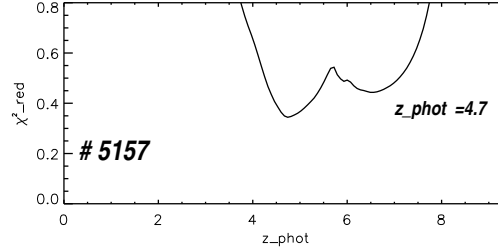
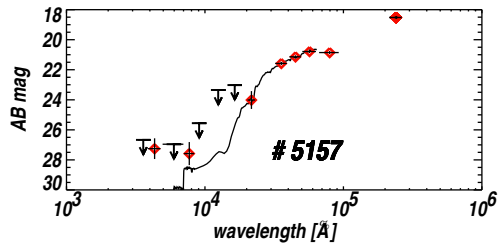
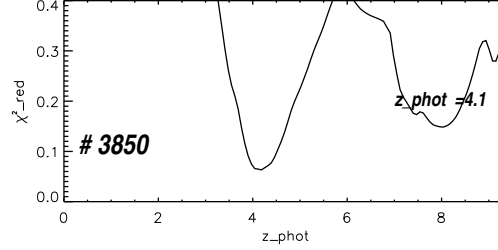
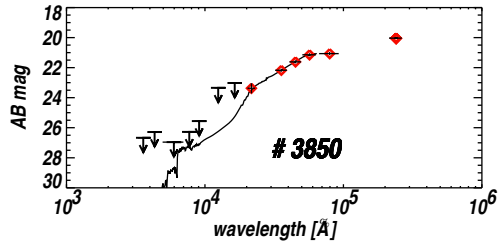
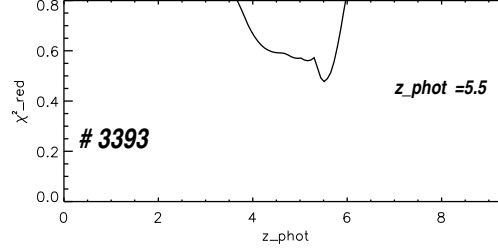
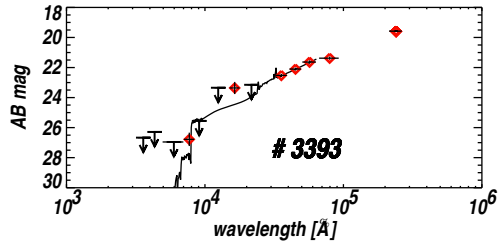
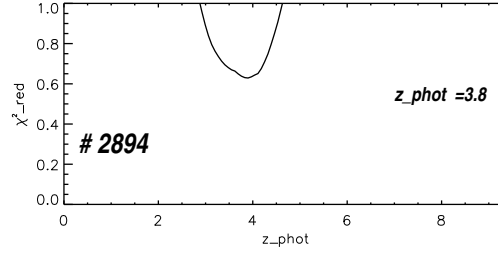
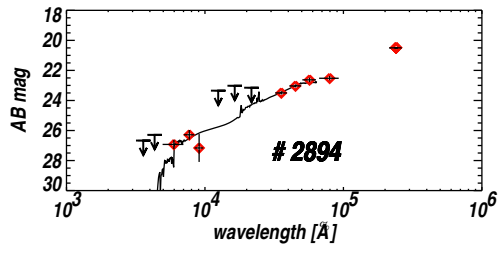


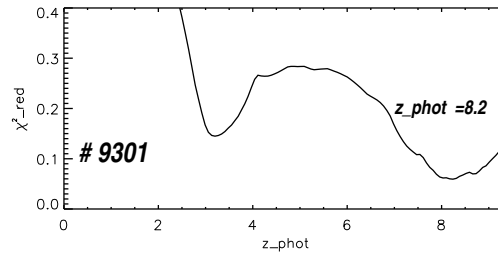
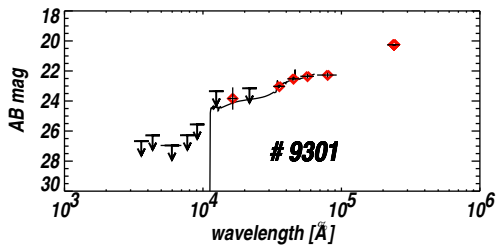
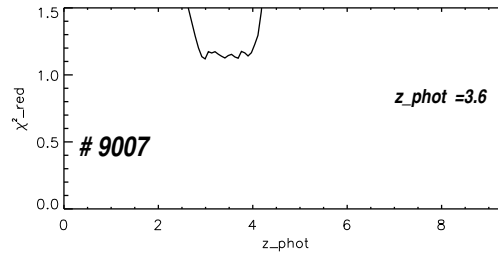
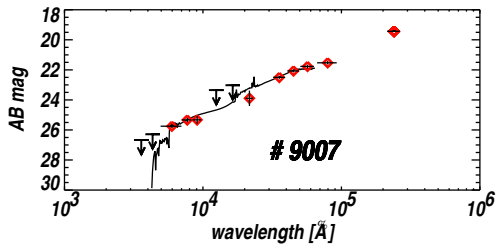
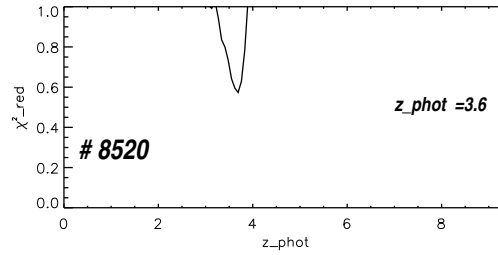
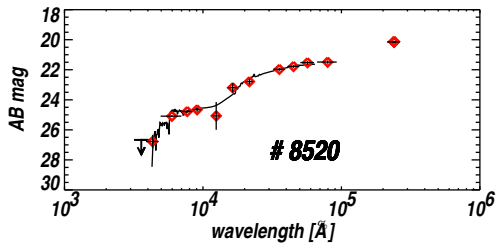
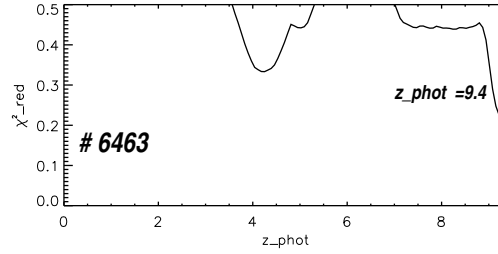
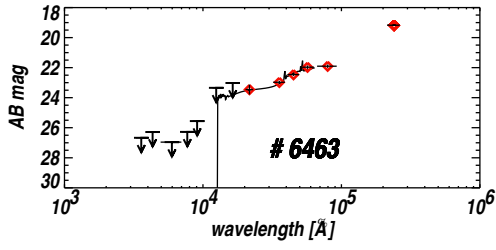
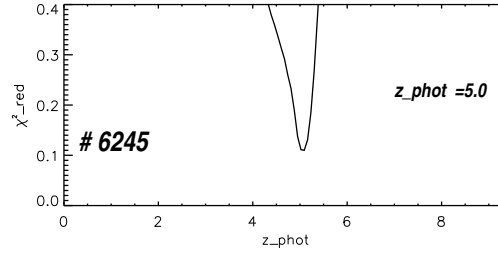
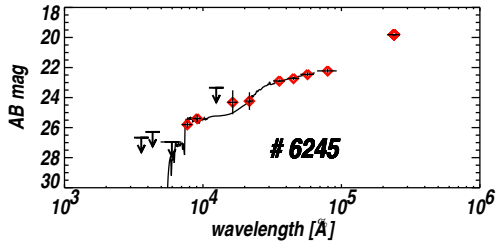
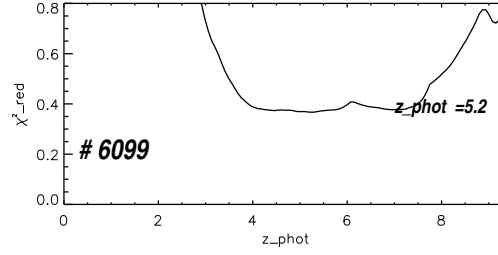
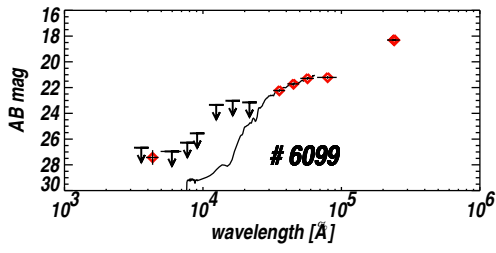




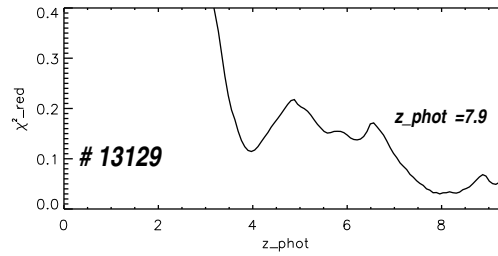
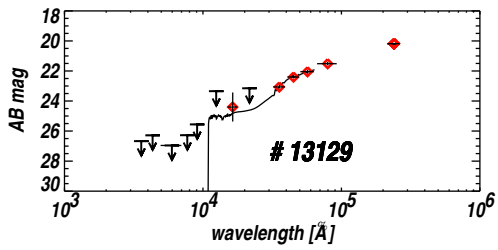
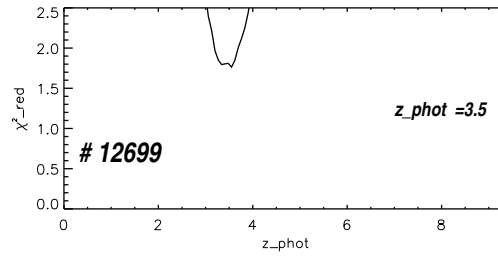
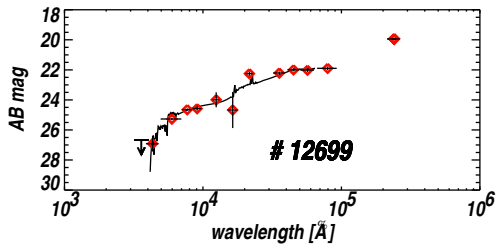
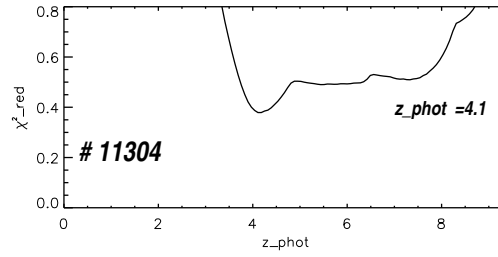
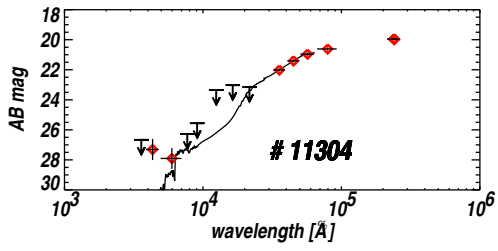
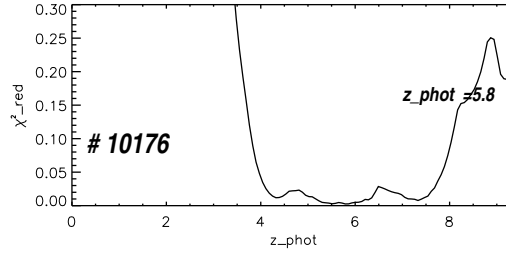
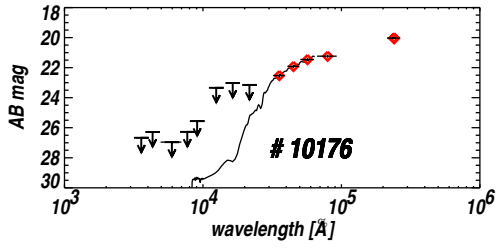
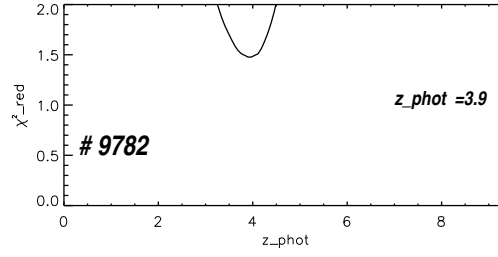
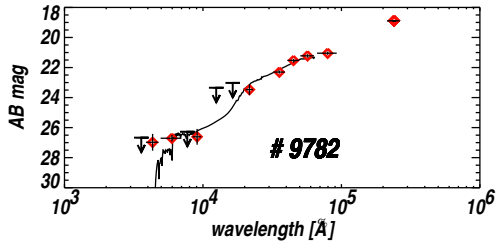
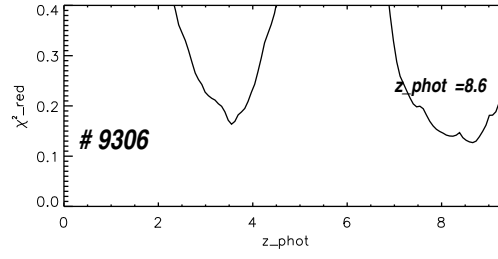
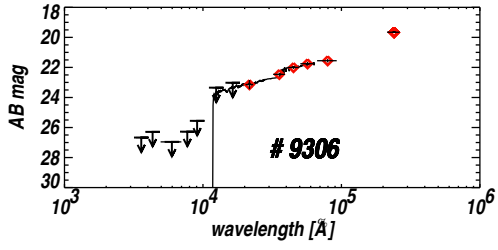


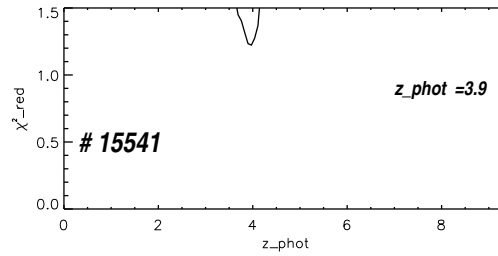
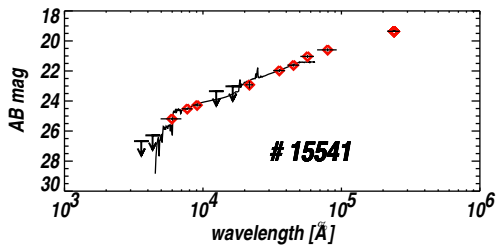
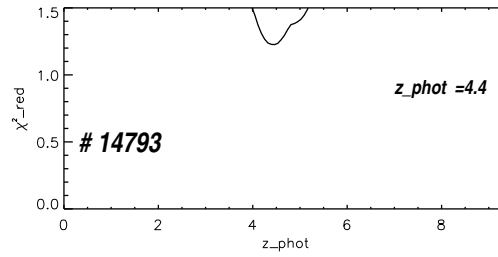
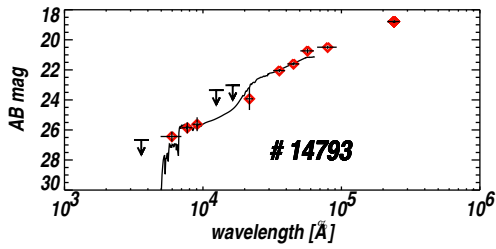
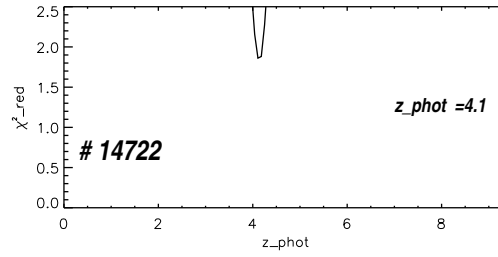
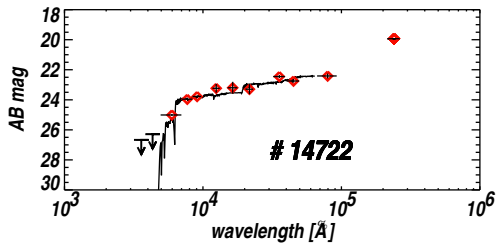
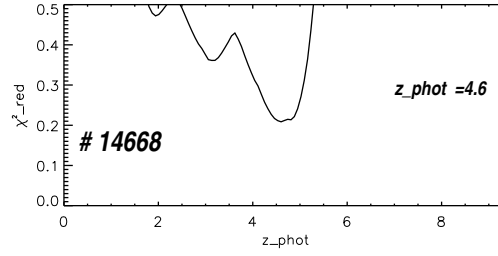
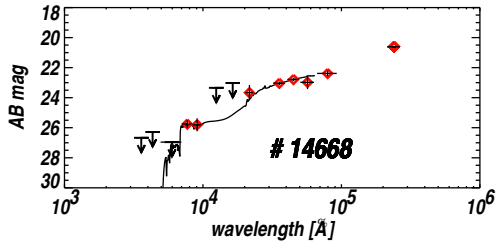
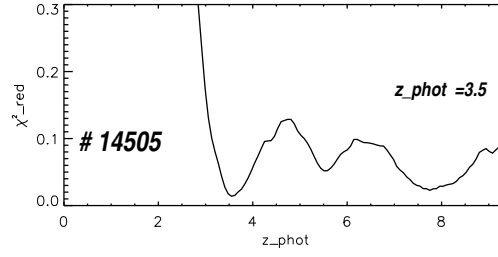
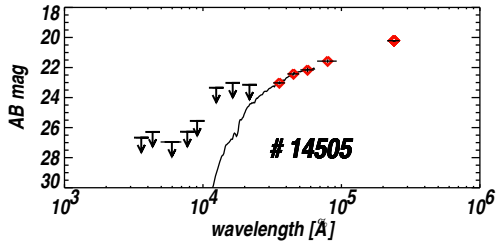
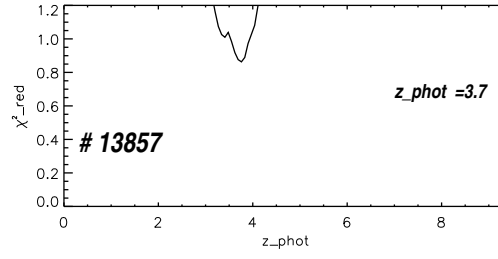
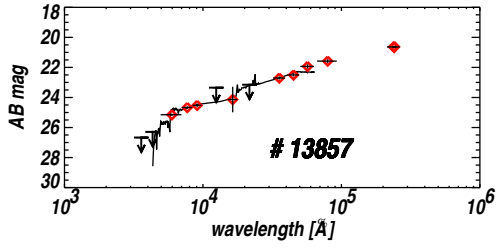
**Fig. 14.** Spectral Energy Distributions of MIPS-d galaxies of our final high- $z$  sample (on the left panels), and the correspondent  $\chi^2_{red}$  distributions as a function of redshift (right panels) in 90% confidence intervals. For each candidate the most probable redshifts (first and second redshift solutions :  $z_{phot}$  and  $z_{phot2}$ ) and the  $\chi^2_{red}$  values with the respective probability are also labeled. See also Tab. 4.

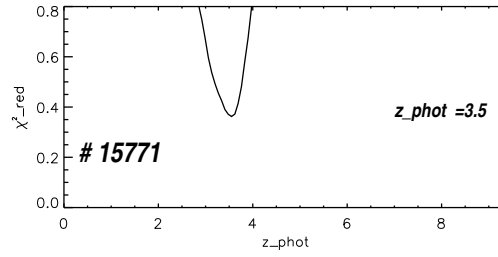
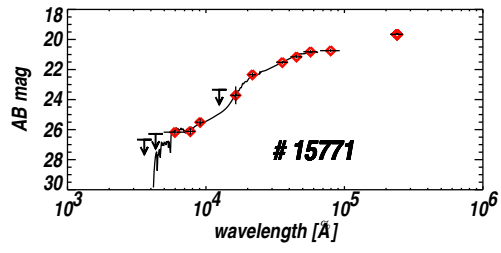
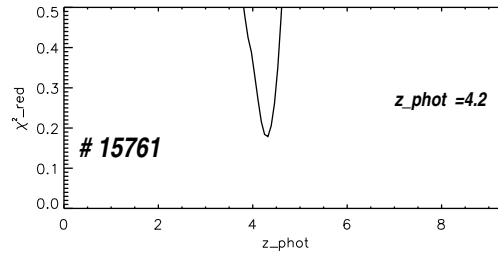
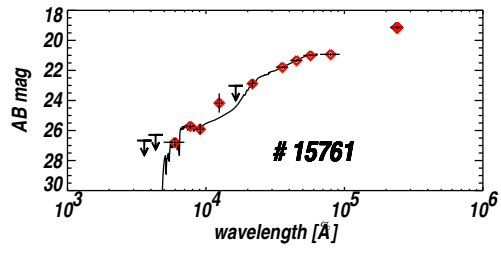




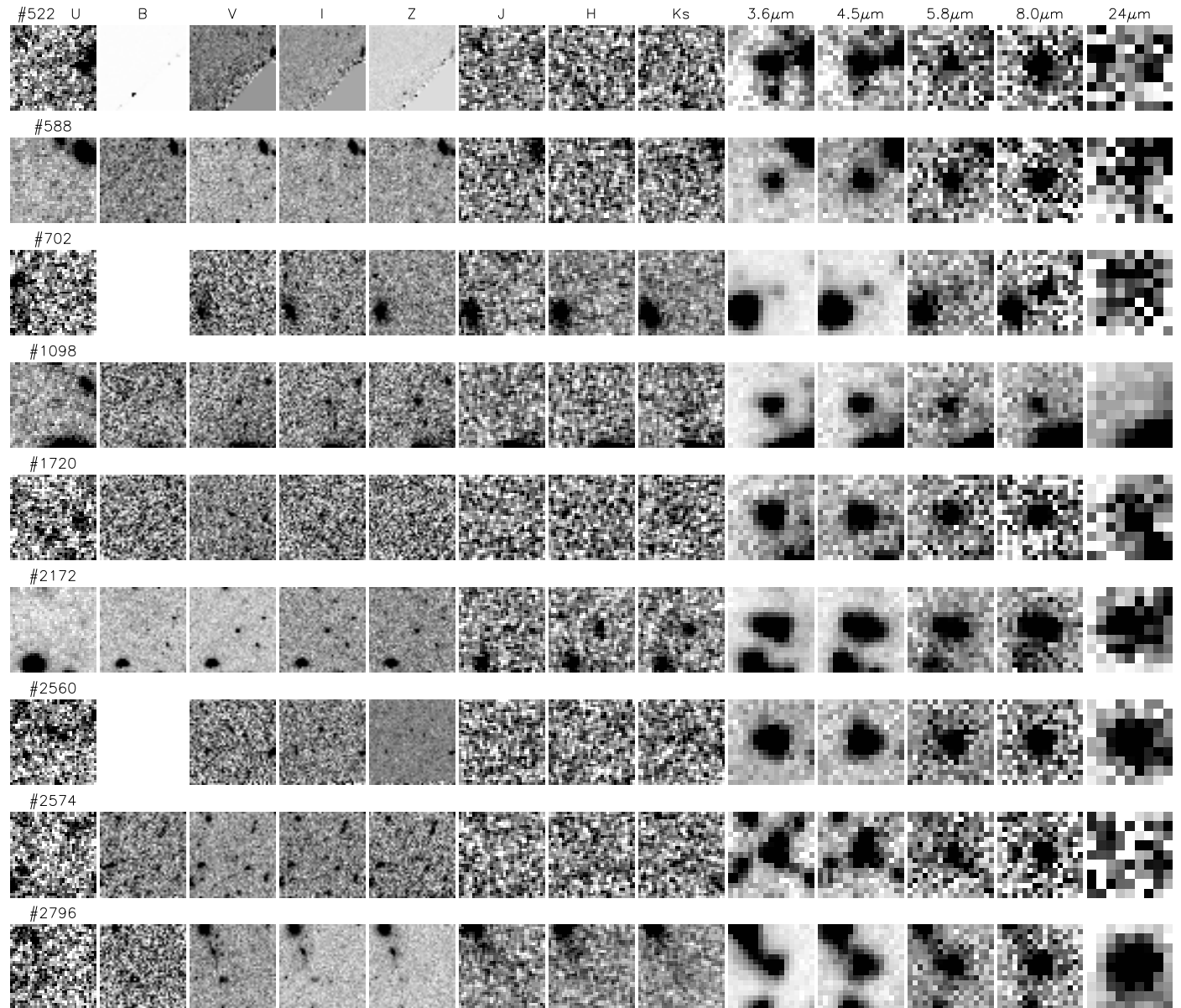


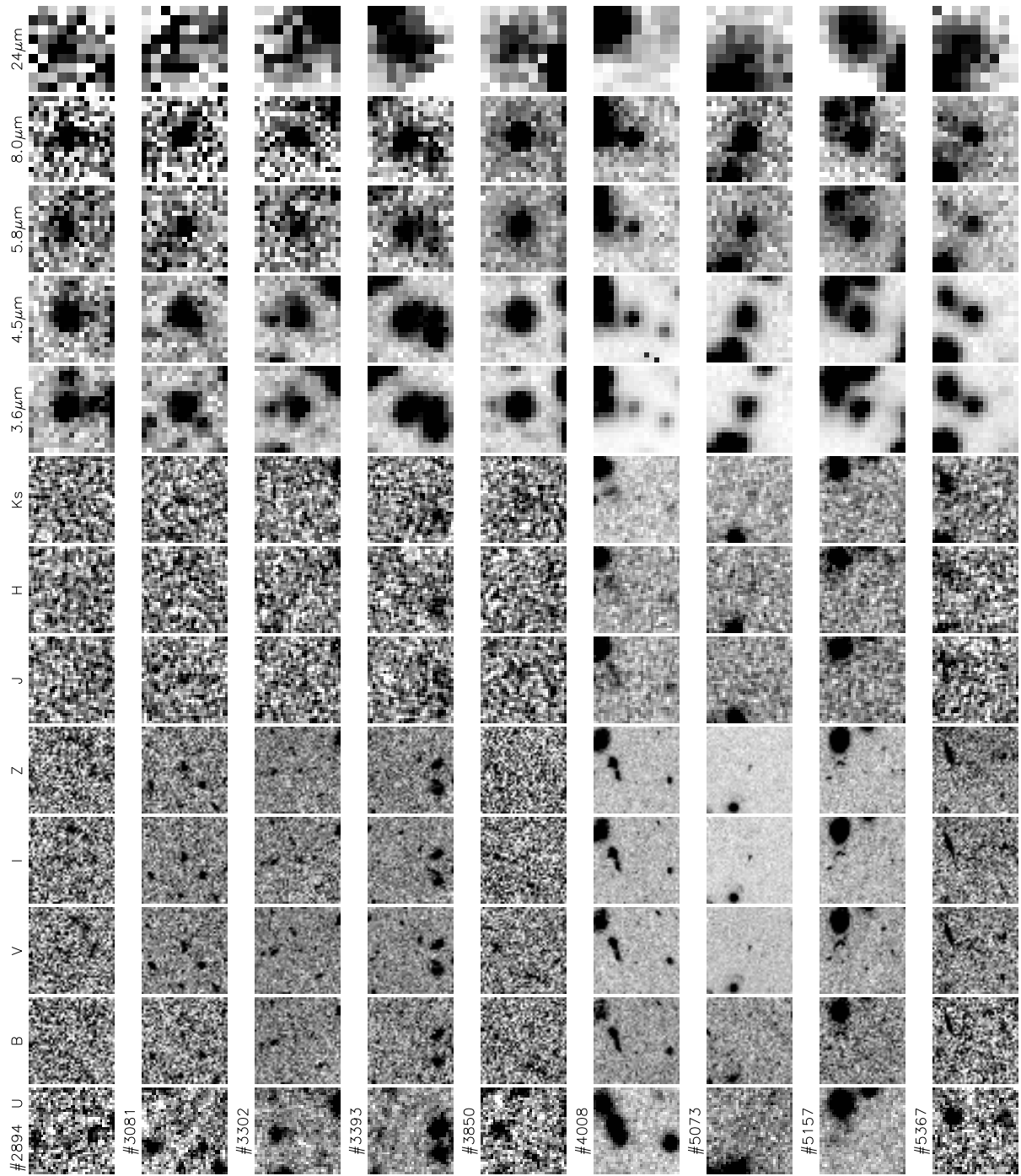


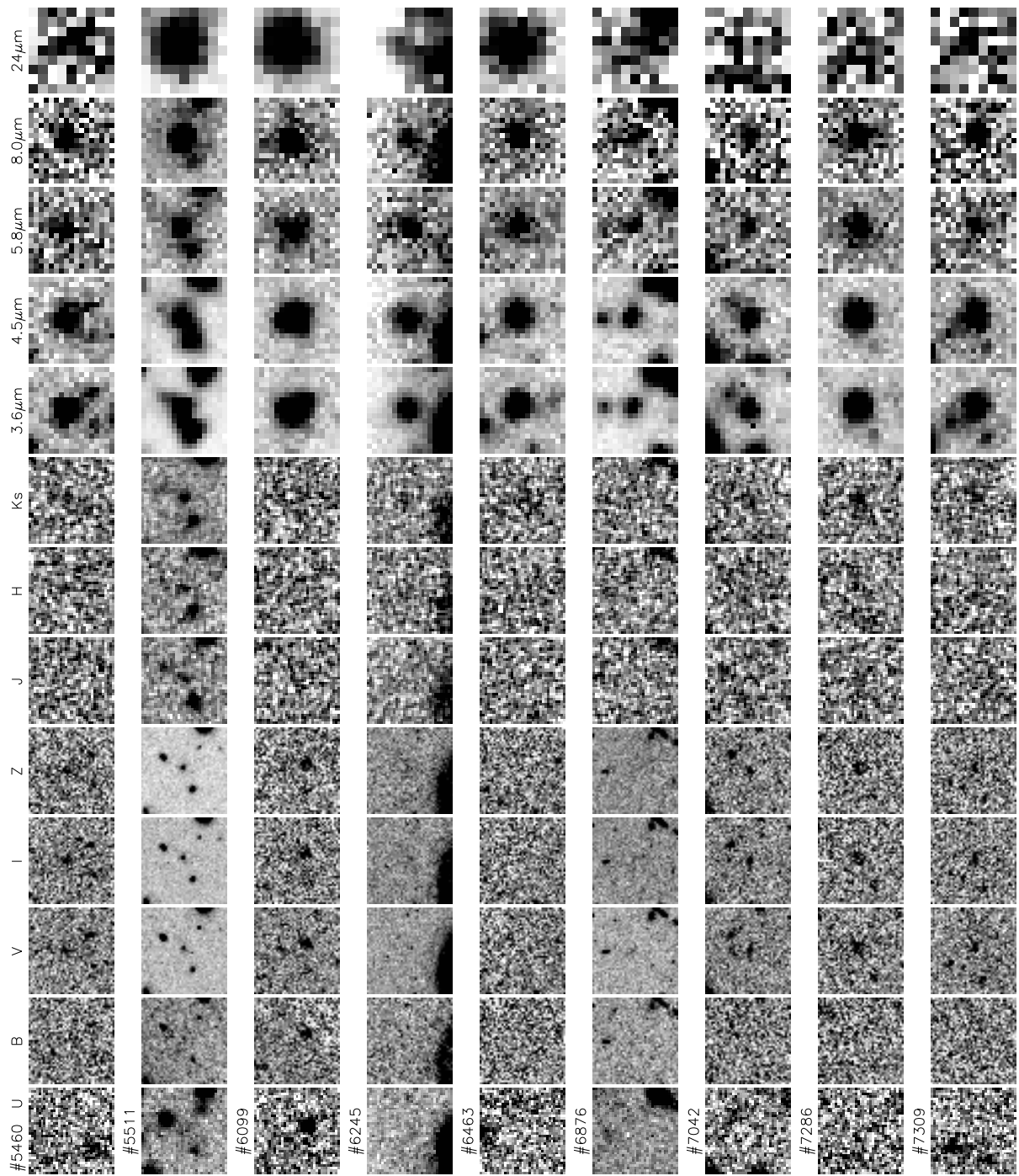


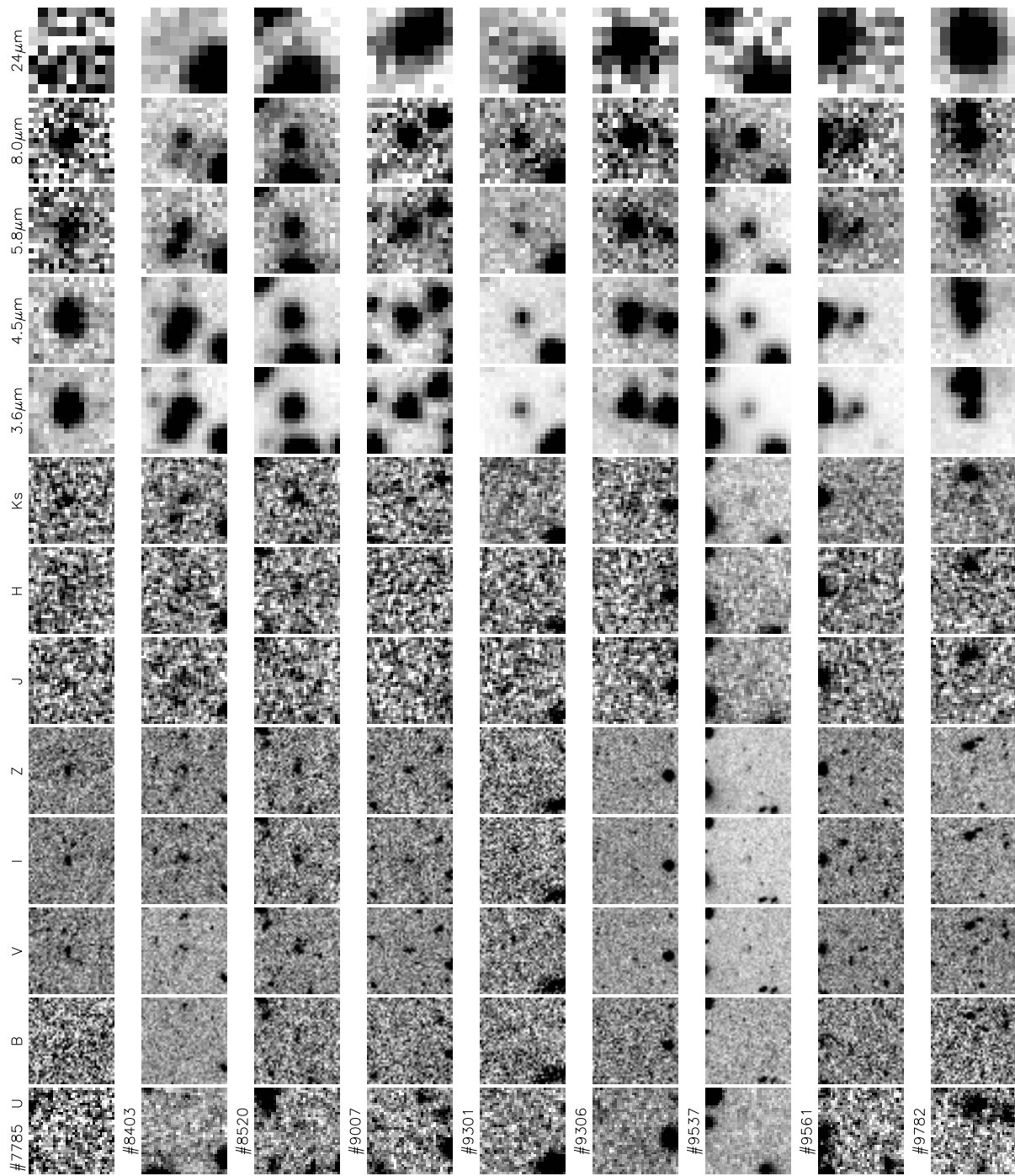


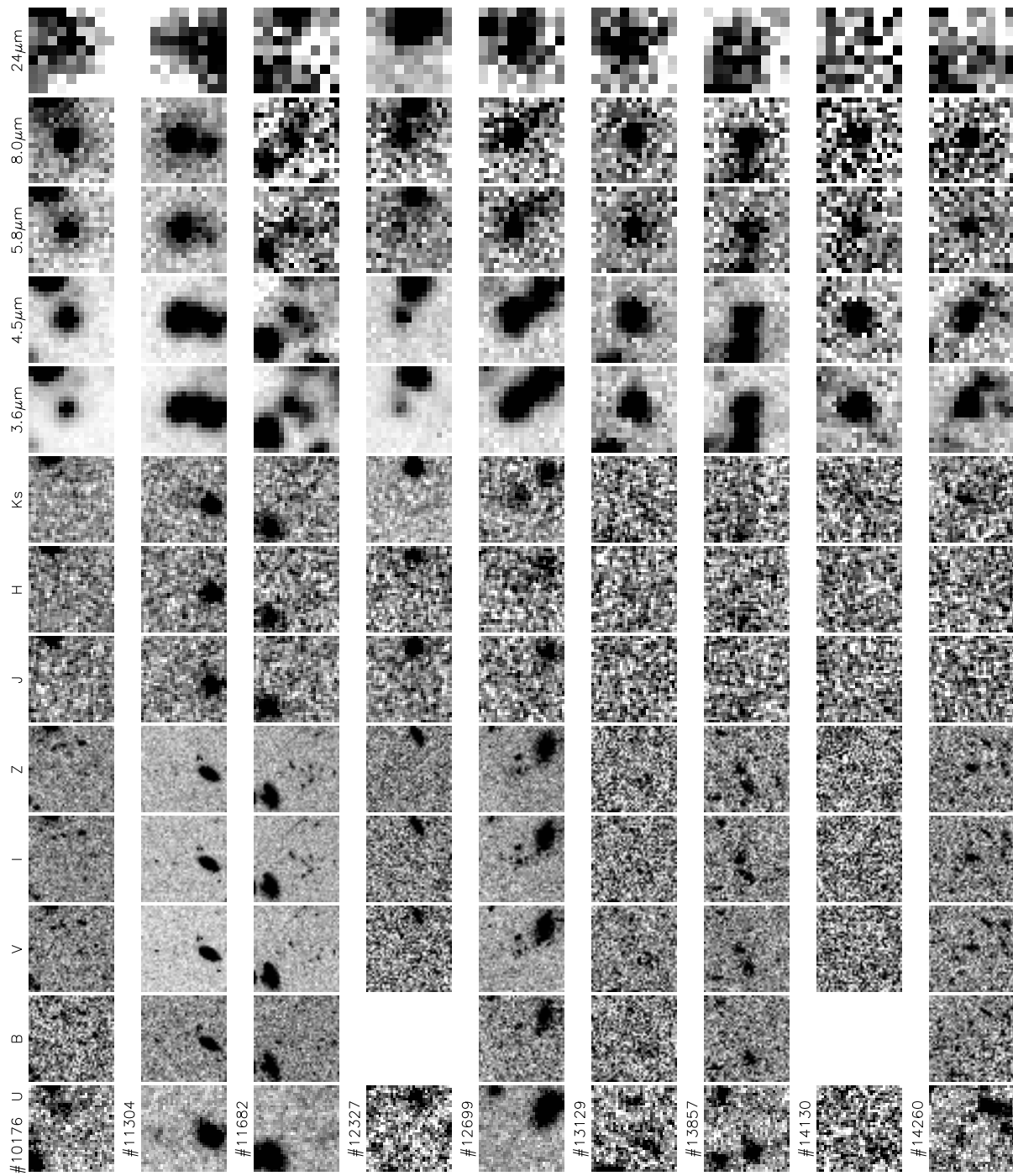
**Fig. 15.** Multi-wavelength images of the fifty-three galaxies of the final sample (MIPS-d+MIPS-u). The cut-outs have a size of  $10'' \times 10''$ . North is up, East is at left.













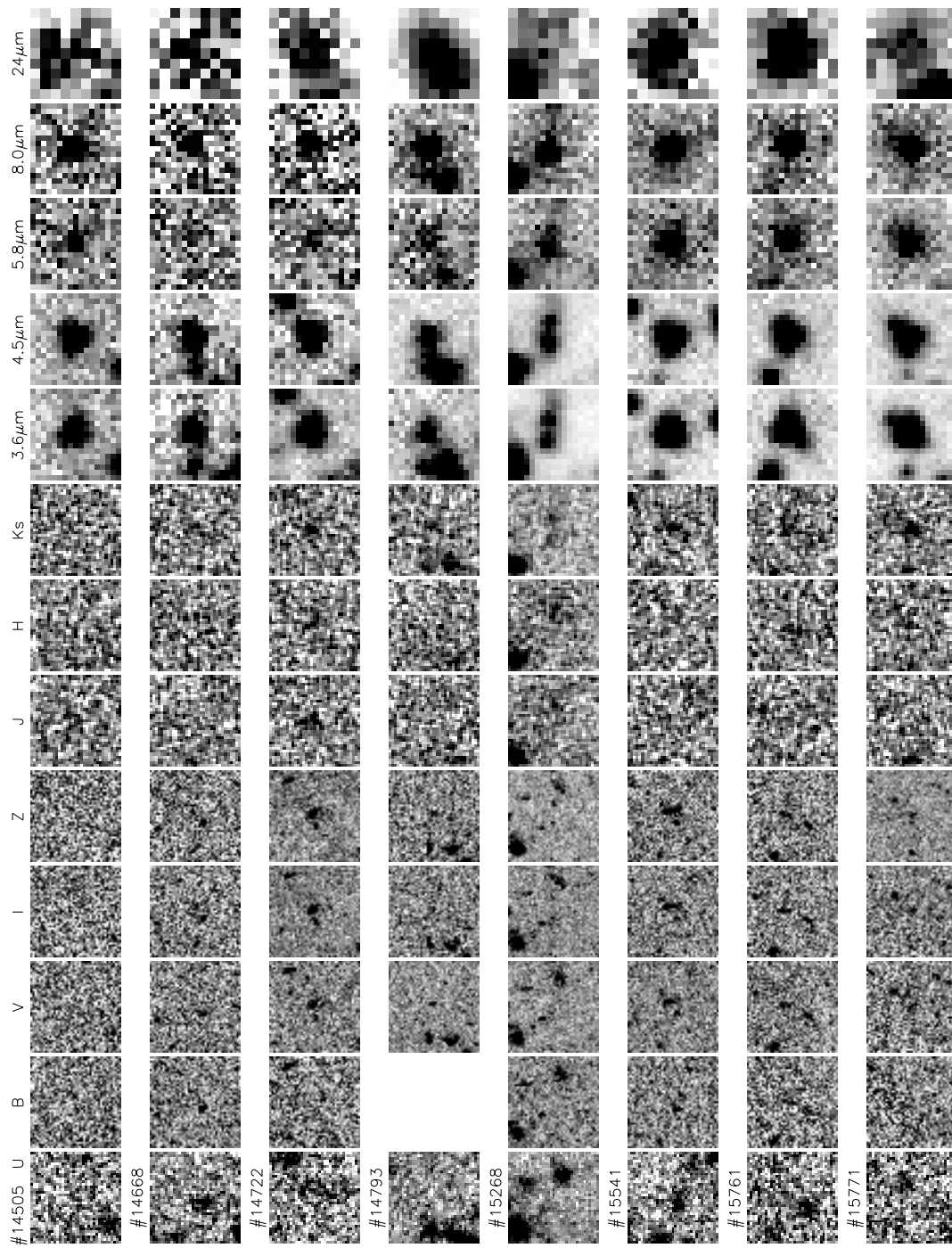


**Table 6.** Multi-band photometry for the final sample of 44 candidates at  $z \geq 3.5$ . The coordinates reported here are from the *Spitzer* data-set.

ID	<i>U</i>	<i>B</i>	<i>V</i>	<i>i</i>	<i>z</i>	<i>J</i>	<i>H</i>	<i>Ks</i>	<i>m</i> <sub>3,6</sub>	<i>m</i> <sub>4,5</sub>	<i>m</i> <sub>5,8</sub>	<i>m</i> <sub>8,0</sub>	<i>m</i> <sub>24</sub>	RA	Dec
# 522	> 26.7	> 26.3	26.485	26.980	> 25.5	> 23.3	> 23.0	> 23.1	23.288	22.895	22.517	21.583	> 20.6	12:36:27.2	62:06:06.1
# 588	> 26.7	27.774	27.187	26.210	> 25.5	> 23.3	> 23.0	> 23.1	23.379	22.960	22.274	21.836	20.218	12:36:32.7	62:06:21.8
# 702	> 26.7	---	> 26.9	> 26.3	> 25.5	> 23.3	> 23.0	> 23.1	---	22.964	22.857	22.254	20.081	12:36:15.7	62:06:43.4
# 1098	> 26.7	26.968	25.998	24.907	24.317	> 23.3	23.242	23.127	22.422	22.465	22.065	21.807	> 20.6	12:36:36.8	62:07:14.0
# 1720	> 26.7	> 26.3	26.397	25.778	26.033	> 23.3	> 23.0	23.021	22.954	22.611	22.354	22.218	20.161	12:36:51.0	62:08:29.8
# 2172	> 26.7	27.262	25.325	24.536	24.243	> 23.3	23.187	22.482	21.360	21.118	20.898	20.928	19.156	12:36:13.3	62:09:02.0
# 2560	> 26.7	---	> 26.9	> 26.3	> 25.5	> 23.3	> 23.0	23.222	21.999	21.587	21.227	21.137	18.527	12:35:53.0	62:09:30.2
# 2574	> 26.7	> 26.3	26.722	26.810	26.070	> 23.3	> 23.0	23.778	22.958	22.559	22.510	22.183	> 20.6	12:36:04.7	62:09:25.5
# 2796	> 26.7	> 26.3	> 26.9	> 26.3	> 25.5	> 23.3	> 23.0	22.404	21.869	21.528	21.167	21.227	18.029	12:36:03.1	62:09:47.5
# 2894	> 26.7	> 26.3	26.926	26.256	27.044	> 23.3	> 23.0	> 23.1	23.399	22.997	22.608	22.521	20.496	12:37:10.0	62:09:56.4
# 3081	> 26.7	27.283	25.263	24.600	24.272	24.240	> 23.0	> 23.1	22.859	22.638	---	22.480	> 20.6	12:36:44.4	62:10:03.9
# 3302	> 26.7	> 26.3	27.155	26.106	25.940	> 23.3	> 23.0	> 23.1	22.834	22.638	22.146	22.169	> 20.6	12:35:59.9	62:10:08.4
# 3393	> 26.7	> 26.3	> 26.9	26.751	> 25.5	> 23.3	23.329	> 23.1	22.423	22.064	21.615	21.376	19.581	12:37:19.5	62:10:21.4
# 3850	> 26.7	> 26.3	> 26.9	> 26.3	> 25.5	> 23.3	> 23.0	23.202	22.073	21.579	21.125	21.066	20.037	12:37:12.5	62:10:36.1
# 4008	> 26.7	> 26.3	> 26.9	> 26.3	> 25.5	> 23.3	> 23.0	23.330	---	22.069	21.817	21.405	> 20.6	12:36:53.7	62:11:12.9
# 5073	> 26.7	> 26.3	26.382	25.038	25.135	> 23.3	23.058	23.489	22.107	21.831	21.602	21.165	> 20.6	12:36:36.1	62:11:54.7
# 5157	> 26.7	27.265	> 26.9	27.550	> 25.5	> 23.3	> 23.0	23.846	21.479	21.102	20.764	20.856	18.519	12:36:37.5	62:11:57.2
# 5367	> 26.7	27.241	27.154	26.063	25.954	> 23.3	> 23.0	> 23.1	22.729	22.373	21.895	21.745	20.189	12:37:18.9	62:12:17.9
# 5460	> 26.7	> 26.3	25.754	24.742	24.932	> 23.3	24.431	24.036	23.019	22.691	22.781	22.567	> 20.6	12:36:31.3	62:12:18.3
# 5511	> 26.7	27.209	25.492	24.543	23.806	24.163	22.865	22.320	21.429	21.444	21.219	20.221	18.084	12:36:37.1	62:12:31.1
# 6099	> 26.7	27.438	> 26.9	> 26.3	> 25.5	> 23.3	> 23.0	> 23.1	22.129	21.678	21.269	21.209	18.305	12:36:08.6	62:12:51.2
# 6245	> 26.7	> 26.3	> 26.9	25.766	25.270	> 23.3	24.283	24.065	22.791	22.688	22.433	22.222	19.809	12:37:20.6	62:13:00.2
# 6463	> 26.7	> 26.3	> 26.9	> 26.3	> 25.5	> 23.3	> 23.0	23.287	22.875	22.426	21.948	21.903	19.177	12:37:02.5	62:13:02.6
# 6876	> 26.7	> 26.3	26.322	26.938	> 25.5	> 23.3	> 23.0	> 23.1	23.042	22.801	22.468	22.386	> 20.6	12:36:30.4	62:13:33.0
# 7042	> 26.7	> 26.3	25.418	24.665	24.685	> 23.3	> 23.0	23.463	23.224	22.992	23.337	23.059	> 20.6	12:37:25.5	62:13:39.8
# 7286	> 26.7	27.443	25.467	26.915	24.953	24.288	24.464	22.810	22.519	22.265	21.941	22.033	> 20.6	12:37:09.5	62:13:50.3
# 7309	> 26.7	27.718	25.498	24.823	24.915	> 23.3	24.377	23.068	23.031	22.875	23.306	22.830	> 20.6	12:36:41.6	62:13:50.1
# 7785	> 26.7	27.099	24.698	23.850	23.618	25.240	23.265	23.026	22.584	22.616	22.637	22.473	> 20.6	12:36:55.9	62:14:12.5
# 8403	> 26.7	> 26.3	25.844	24.729	24.927	23.792	22.877	22.841	22.198	21.971	22.106	21.684	> 20.6	12:37:03.8	62:14:51.6
# 8520	> 26.7	26.790	25.090	24.743	24.539	24.971	23.162	22.617	21.867	21.739	21.504	21.488	20.144	12:36:45.1	62:14:48.8
# 9007	> 26.7	> 26.3	25.750	25.303	25.209	> 23.3	> 23.0	23.721	22.399	22.033	21.749	21.528	19.433	12:37:34.7	62:15:15.8
# 9301	> 26.7	> 26.3	> 26.9	> 26.3	> 25.5	> 23.3	23.802	> 23.1	22.924	22.484	22.332	22.270	20.255	12:38:03.6	62:15:30.5
# 9306	> 26.7	> 26.3	> 26.9	> 26.3	> 25.5	> 23.3	> 23.0	22.973	22.360	21.967	21.735	21.555	19.661	12:37:33.8	62:15:32.1
# 9537	> 26.7	> 26.3	26.557	25.606	25.600	> 23.3	> 23.0	22.824	22.133	21.873	21.650	21.485	> 20.6	12:36:39.4	62:15:42.8
# 9561	> 26.7	> 26.3	26.310	25.492	26.253	> 23.3	> 23.0	23.056	---	22.686	22.597	22.463	> 20.6	12:37:52.7	62:15:49.3
# 9782	> 26.7	26.988	26.705	> 26.3	26.493	> 23.3	> 23.0	23.298	22.203	21.487	21.199	21.046	18.889	12:37:39.5	62:15:59.0
# 10176	> 26.7	> 26.3	> 26.9	> 26.3	> 25.5	> 23.3	> 23.0	> 23.1	22.428	21.882	21.439	21.237	20.034	12:36:22.0	62:16:16.2
# 11304	> 26.7	27.318	27.906	> 26.3	> 25.5	> 23.3	> 23.0	> 23.1	21.918	21.373	20.939	20.617	19.959	12:36:31.9	62:17:14.8
# 11682	> 26.7	> 26.3	26.464	25.416	25.536	> 23.3	> 23.0	24.296	22.702	22.682	22.455	22.507	> 20.6	12:37:39.2	62:17:36.8
# 12327	> 26.7	---	> 26.9	26.574	> 25.5	> 23.3	> 23.0	24.705	22.645	22.189	22.091	21.367	> 20.6	12:38:05.4	62:18:16.4
# 12699	> 26.7	26.925	25.271	24.616	24.460	23.892	24.640	22.082	22.107	21.959	21.996	21.895	19.942	12:37:24.0	62:18:33.7
# 13129	> 26.7	> 26.3	> 26.9	> 26.3	> 25.5	> 23.3	24.368	> 23.1	22.963	22.364	22.029	21.515	20.186	12:37:28.1	62:19:20.5
# 13857	> 26.7	> 26.3	25.150	24.638	24.404	> 23.3	24.107	> 23.1	22.605	22.465	21.913	21.578	20.637	12:37:08.8	62:22:02.2
# 14130	> 26.7	---	> 26.9	25.899	26.511	> 23.3	> 23.0	23.387	23.048	22.900	22.846	22.596	> 20.6	12:37:36.3	62:21:25.3
# 14260	> 26.7	> 26.3	25.352	24.183	23.941	23.682	24.668	22.678	22.552	22.680	22.814	22.647	> 20.6	12:37:13.0	62:21:11.4
# 14505	> 26.7	> 26.3	> 26.9	> 26.3	> 25.5	> 23.3	> 23.0	> 23.1	22.924	22.388	22.140	21.573	20.211	12:36:44.0	62:19:38.8
# 14668	> 26.7	> 26.3	> 26.9	25.723	25.684	> 23.3	> 23.0	23.497	22.936	22.749	22.956	22.385	20.610	12:37:12.3	62:23:03.4
# 14722	> 26.7	> 26.3	25.010	23.929	23.658	23.133	23.167	23.125	22.352	22.714	---	22.414	19.934	12:37:11.5	62:21:55.8
# 14793	> 26.7	---	26.436	25.824	25.501	> 23.3	> 23.0	23.757	21.952	21.566	20.716	20.492	18.787	12:36:58.9	62:22:15.3
# 15268	> 26.7	> 26.3	> 26.9	25.710	> 25.5	> 23.3	> 23.0	> 23.1	22.790	21.887	21.316	21.071	> 20.6	12:37:09.6	62:22:02.5
# 15541	> 26.7	> 26.3	25.185	24.487	24.155	> 23.3	> 23.0	22.753	21.874	21.573	21.010	20.595	19.359	12:37:11.9	62:22:12.4
# 15761	> 26.7	> 26.3	26.783	25.670	25.788	24.071	> 23.0	22.707	21.688	21.299	20.985	20.931	19.140	12:36:55.3	62:21:07.9
# 15771	> 26.7	> 26.3	26.170	26.087	25.386	> 23.3	23.687	22.170	21.418	21.117	20.795	20.743	19.659	12:37:01.5	62:20:25.3

## References

- Alexander, D. M., Bauer, F. E., Brandt, W. N., et al. 2003, *AJ*, 126, 539
- Alonso-Herrero, A., Pérez-González, P. G., Alexander, D. M., et al. 2006, *ApJ*, 640, 167
- Baldry, I. K., Glazebrook, K., Brinkmann, J., et al. 2004, *ApJ*, 600, 681
- Berta, S., Lonsdale, C. J., Siana, B., et al. 2007, *A&A*, 467, 565
- Bertin, E. & Arnouts, S. 1996, *A&AS*, 117, 393
- Bertoldi, F., Menten, K. M., Kreysa, E., Carilli, C. L., & Owen, F. 2000, *astro-ph/0010553*
- Bolzonella, M., Miralles, J.-M., & Pelló, R. 2000, *A&A*, 363, 476
- Borys, C., Chapman, S., Halpern, M., & Scott, D. 2003, *MNRAS*, 344, 385
- Bower, R. G., Benson, A. J., Malbon, R., et al. 2006, *MNRAS*, 370, 645
- Brammer, G. B. & van Dokkum, P. G. 2007, *ApJ*, 654, L107
- Bruzual, G. & Charlot, S. 2003, *MNRAS*, 344, 1000
- Bruzual A, G. 2007, *astro-ph/0703052*
- Bunker, A. J., Stanway, E. R., Ellis, R. S., McMahon, R. G., & McCarthy, P. J. 2003, *MNRAS*, 342, L47
- Calzetti, D., Armus, L., Bohlin, R. C., et al. 2000, *ApJ*, 533, 682
- Capak, P., Cowie, L. L., Hu, E. M., et al. 2004, *AJ*, 127, 180
- Chabrier, G. 2003, *PASP*, 115, 763
- Chapman, S. C., Blain, A. W., Smail, I., & Ivison, R. J. 2005, *ApJ*, 622, 772
- Chary, R. & Elbaz, D. 2001, *ApJ*, 556, 562
- Chary, R.-R., Teplitz, H. I., Dickinson, M. E., et al. 2007, *ApJ*, 665, 257
- Chen, H.-W. & Marzke, R. O. 2004, *ApJ*, 615, 603
- Cimatti, A., Cassata, P., Pozzetti, L., et al. 2008, *A&A*, 482, 21
- Cimatti, A., Daddi, E., Renzini, A., et al. 2004, *Nature*, 430, 184
- Coleman, G. D., Wu, C.-C., & Weedman, D. W. 1980, *ApJS*, 43, 393
- Cowie, L. L., Barger, A. J., Hu, E. M., Capak, P., & Songaila, A. 2004, *AJ*, 127, 3137
- Daddi, E., Dannerbauer, H., Stern, D., et al. 2008, *arXiv:0810.3108*
- Daddi, E., Dickinson, M., Morrison, G., et al. 2007, *ApJ*, 670, 156
- Daddi, E., Renzini, A., Pirzkal, N., et al. 2005, *ApJ*, 626, 680
- Dannerbauer, H., Walter, F., & Morrison, G. 2008, *ApJ*, 673, L127
- Dawson, S., Stern, D., Bunker, A. J., Spinrad, H., & Dey, A. 2001, *AJ*, 122, 598
- Dickinson, M. 1998, in *The Hubble Deep Field*, ed. M. Livio, S. M. Fall, & P. Madau, 219–+
- Dickinson, M., Giavalisco, M., & The Goods Team. 2003, in *The Mass of Galaxies at Low and High Redshift*, ed. R. Bender & A. Renzini, 324–+
- Dickinson, M., Stern, D., Giavalisco, M., et al. 2004, *ApJ*, 600, L99
- Donley, J. L., Rieke, G. H., Pérez-González, P. G., Rigby, J. R., & Alonso-Herrero, A. 2007, *ApJ*, 660, 167
- Drory, N., Bender, R., Feulner, G., et al. 2004, *ApJ*, 608, 742
- Drory, N., Salvato, M., Gabasch, A., et al. 2005, *ApJ*, 619, L131
- Dunlop, J. S., Cirasuolo, M., & McLure, R. J. 2007, *MNRAS*, 376, 1054
- Eyles, L. P., Bunker, A. J., Ellis, R. S., et al. 2007, *MNRAS*, 374, 910
- Eyles, L. P., Bunker, A. J., Stanway, E. R., et al. 2005, *MNRAS*, 364, 443
- Fazio, G. G., Hora, J. L., Allen, L. E., et al. 2004, *ApJS*, 154, 10
- Fontana, A., Pozzetti, L., Donnarumma, I., et al. 2004, *A&A*, 424, 23
- Fontana, A., Salimbeni, S., Grazian, A., et al. 2006, *A&A*, 459, 745
- Franx, M., Labbé, I., Rudnick, G., et al. 2003, *ApJ*, 587, L79
- Giavalisco, M., Dickinson, M., Ferguson, H. C., et al. 2004a, *ApJ*, 600, L103
- Giavalisco, M., Ferguson, H. C., Koekemoer, A. M., et al. 2004b, *ApJ*, 600, L93
- Greve, T. R., Bertoldi, F., Smail, I., et al. 2005, *MNRAS*, 359, 1165
- Greve, T. R., Pope, A., Scott, D., et al. 2008, *MNRAS*, 389, 1489
- Guhathakurta, P., Tyson, J. A., & Majewski, S. R. 1990, *ApJ*, 357, L9
- Holland, W. S., Robson, E. I., Gear, W. K., et al. 1999, *MNRAS*, 303, 659
- Kannappan, S. J. & Gawiser, E. 2007, *ApJ*, 657, L5
- Kauffmann, G. & Charlot, S. 1998, *MNRAS*, 297, L23+
- Kennicutt, Jr., R. C. 1998, *ARA&A*, 36, 189
- Kriek, M., van Dokkum, P. G., Franx, M., et al. 2006, *ApJ*, 649, L71
- Kroupa, P. 2001, *MNRAS*, 322, 231
- Labbé, I., Huang, J., Franx, M., et al. 2005, *ApJ*, 624, L81
- Lejeune, T., Cuisinier, F., & Buser, R. 1997, *A&AS*, 125, 229
- Lilly, S. J., Eales, S. A., Gear, W. K. P., et al. 1999, *ApJ*, 518, 641
- Madau, P. 1995, *ApJ*, 441, 18
- Maraston, C. 2005, in *Multiwavelength Mapping of Galaxy Formation and Evolution*, ed. A. Renzini & R. Bender, 290–+
- Maraston, C., Daddi, E., Renzini, A., et al. 2006, *ApJ*, 652, 85
- McCarthy, P. J., Le Borgne, D., Crampton, D., et al. 2004, *ApJ*, 614, L9
- McLure, R. J., Cirasuolo, M., Dunlop, J. S., et al. 2006, *MNRAS*, 372, 357
- Mobasher, B., Dickinson, M., Ferguson, H. C., et al. 2005, *ApJ*, 635, 832
- Muller, G. P., Reed, R., Armandroff, T., Boroson, T. A., & Jacoby, G. H. 1998, in *Presented at the Society of Photo-Optical Instrumentation Engineers (SPIE) Conference*, Vol. 3355, Proc. SPIE Vol. 3355, p. 577-585, *Optical Astronomical Instrumentation*, Sandro D'Odorico; Ed., ed. S. D'Odorico, 577–585
- Night, C., Nagamine, K., Springel, V., & Hernquist, L. 2006, *MNRAS*, 366, 705
- Papovich, C., Rudnick, G., Le Floch, E., et al. 2007, *ApJ*, 668, 45
- Perera, T. A., Chapin, E. L., Austermann, J. E., et al. 2008, *MNRAS*, 391, 1227
- Pope, A., Borys, C., Scott, D., et al. 2005, *MNRAS*, 358, 149
- Pope, A., Scott, D., Dickinson, M., et al. 2006, *MNRAS*, 370, 1185
- Pozzetti, L., Bolzonella, M., Lamareille, F., et al. 2007, *A&A*, 474, 443
- Reddy, N. A., Steidel, C. C., Erb, D. K., Shapley, A. E., & Pettini, M. 2006, *ApJ*, 653, 1004
- Rieke, G. H., Young, E. T., Engelbracht, C. W., et al. 2004, *ApJS*, 154, 25
- Rigby, J. R., Marcillac, D., Egami, E., et al. 2008, *ApJ*, 675, 262
- Rodighiero, G., Cimatti, A., Franceschini, A., et al. 2007, *A&A*, 470, 21
- Rodighiero, G., Lari, C., Pozzi, F., et al. 2006, *MNRAS*, 371, 1891
- Saracco, P., Longhetti, M., Severgnini, P., et al. 2005, *MNRAS*, 357, L40
- Sawicki, M. 2002, *AJ*, 124, 3050
- Scott, S. E., Fox, M. J., Dunlop, J. S., et al. 2002, *MNRAS*, 331, 817
- Spinrad, H., Stern, D., Bunker, A., et al. 1998, *AJ*, 116, 2617
- Stanway, E. R., Bunker, A. J., McMahon, R. G., et al. 2004, *ApJ*, 607, 704
- Stark, D. P., Bunker, A. J., Ellis, R. S., Eyles, L. P., & Lacy, M. 2007, *ApJ*, 659, 84
- Steidel, C. C., Adelberger, K. L., Giavalisco, M., Dickinson, M., & Pettini, M. 1999, *ApJ*, 519, 1
- Steidel, C. C., Adelberger, K. L., Shapley, A. E., et al. 2003, *ApJ*, 592, 728
- Steidel, C. C., Giavalisco, M., Pettini, M., Dickinson, M., & Adelberger, K. L. 1996, *ApJ*, 462, L17+
- Steidel, C. C. & Hamilton, D. 1992, *AJ*, 104, 941
- Vanzella, E., Cristiani, S., Dickinson, M., et al. 2008, *A&A*, 478, 83
- Verma, A., Lehnert, M. D., Förster Schreiber, N. M., Bremer, M. N., & Douglas, L. 2007, *MNRAS*, 377, 1024
- Wang, W.-H., Barger, A. J., & Cowie, L. L. 2009, *ApJ*, 690, 319
- Wang, W.-H., Cowie, L. L., van Saders, J., Barger, A. J., & Williams, J. P. 2007, *ApJ*, 670, L89
- Werner, M. W., Roellig, T. L., Low, F. J., et al. 2004, *ApJS*, 154, 1
- Wiklind, T., Dickinson, M., Ferguson, H. C., et al. 2008, *ApJ*, 676, 781
- Wilkins, S. M., Trentham, N., & Hopkins, A. M. 2008, *MNRAS*, 385, 687
- Wilson, G. W., Austermann, J. E., Perera, T. A., et al. 2008, *MNRAS*, 386, 807
- Wirth, G. D., Willmer, C. N. A., Amico, P., et al. 2004, *AJ*, 127, 3121
- Wuyts, S., Labbé, I., Franx, M., et al. 2007, *ApJ*, 655, 51
- Yan, H., Dickinson, M., Eisenhardt, P. R. M., et al. 2004, *ApJ*, 616, 63
- Yan, H., Dickinson, M., Giavalisco, M., et al. 2006, *ApJ*, 651, 24
- Yan, H., Dickinson, M., Giavalisco, M., et al. 2007, in *Astronomical Society of the Pacific Conference Series*, Vol. 380, *Astronomical Society of the Pacific Conference Series*, ed. J. Afonso, H. C. Ferguson, B. Mobasher, & R. Norris, 35–+